Alma Mater Studiorum – Università di Bologna

DOTTORATO DI RICERCA IN

Modellistica fisica per la protezione dell'Ambiente

Ciclo XV°

Settore Concorsuale di afferenza: 02/C1

Settore Scientifico disciplinare: FIS/06

TITOLO TESI

Radar based improvements and diagnosis of the convective capabilities of the COSMO-2 model

Presentata da: Franco Laudanna Del Guerra

Coordinatore Dottorato **Relatore**

Prof. R. Rizzi **Prof. R. Rizzi**

Esame finale anno 2013

Contents

Chapter 1

Introduction

Precipitation constitutes one of the most important meteorological parameters of our habi- tat and influences life in various ways. As an elementary component of the hydrological cycle it provides fresh water and soil moisture which determines the vegetation cover and thus the basis for agriculture. On the other hand, heavy precipitation events carry the po- tential for large damage in the form of flash floods, landslides, avalanches, hail and strong wind gusts. An improved understanding and accurate forecasts of precipitating weather systems is thus not only of scientific interest but also of high socio-economic importance. Despite large efforts to improve the skill of quantitative precipitation forecasts (QPF) progress has been slow in recent years, especially for the warm season which is dominated by convection (Ebert et al., 2003; Fritsch and Carbone, 2004; Weckwerth et al., 2004).

1.1 The challenge of the assimilation of radar data

In the last few years the resolution of numerical weather prediction (NWP) became higher and higher with the progresses of technology and knowledge. As a consequence, a great number of initial data became fundamental for a correct initialization of the models. The potential of radar observations has long been recognized for improving the initial conditions of high-resolution NWP models (Macpherson et al. [2004]), while operational application becomes more frequent.

Assimilation of data is a statistical discipline which aim to combine various bits of information, i.e. a short-term forecast and the most recent observations, given their relative quality (Kalnay [2003]).For this purpose we need to know, at all the grid points, the model error with all the covariances

between the variables. In particular when we are using remote sense observation we should know the error covariance matrix. Keeler and Ellis [2000] derive an error covariance matrix using reflectivity, radial winds and spectrum width, while Berenguer and Zawadzki [2008] have proposed a physically based approach for the derivation of the radar covariance matrix for stratiform precipitation considering the effects of range and of the variability of the drop size distribution making use of disdrometer observations. Germann et al. [2006] derive an error climatology for precipitation estimates, while Sempere-Torres et al. [2008] propose a real time error estimation comparing precipitation estimates against a benchmark, i.e. two different stages of their quality control cascade.

Rossa and Michaelides [2005], Michelson et al. [2004] in the framework of COST 717 promoted significantly quality description of radar data and carried over to the EUMETNET OPERA program (Holleman et al. [2006]). Several approaches have been proposed based on how significant the quality control algorithms impact the observations (Friedrich and Hagen [2004], Fornasiero et al. [2006]).

All these efforts share a detaild knowledge of the radar systems as a prerequisite to derive an error information. Some extra informations are often needed from complementary observations, such as disdrometers (Berenguer and Zawadzki [2008]) or a high-resolution rain gauge network (Germann et al. [2006]).

European countries have a very heterogeneous collection of national and even regional radar networks. The OPERA program (Operational Programme for the Exchange of weather RAdar information) is making a significant effort to harmonize the radar data exchange but a standard for quality characterization has yet to be estabilished. The fact that many NWP centres have recently taken into operations convection-permitting forecast models, many of which assimilate radar data, emphasizes the need for a pragmatic approach to providing quality information which is needed in order to avoid that radar errors degrade the model's initial conditions and, therefore, its forecasts (Rossa and Leuenbeger [2008]).

Many pragmatic approaches have been widely applied and can be as simple as parametrizing the radar data quality with range (Jones and Macpherson [1997]). Geometrical visibility, or height above the surface of the lowest elevation of a pixel would be slightly more sophisticated but this visibility will depend on the atmospheric conditions and, therefore, on the season. (Germann and Joss [2004b]) show that a long-term precipitation accumulation reflects the radar visibility to some detail.

Environmental risks can can be related with various causes: meteorological, seismical, hydrological/hydraulic for example. The last one can be

related with a lot of phenomena, as heavy convective events that can bring to flash flood with damages to infrastructures and loss of human lives. The flash floods have horizontal dimension of 1-20 Km and can be inserted in mesoscale gamma subscale, this scale can be modeled only with Numerical Weather Prediction (NWP) model with the highest resolution as the COSMO-2 model. One of the problems of modeling extreme convective events is related with the atmospheric initial conditions, in fact the scale dimension for the assimilation of atmospheric condition in an high resolution model is about 10 Km, a value too high for a correct representation of convection initial conditions. Assimilation of radar data with his resolution of about of 1 Km every 5 or 10 minutes can be a solution for this problem.

In this contribution a pragmatic and empirical approach to deriving a radar data quality description is proposed to be used in radar data assimilation and more specifically for the latent heat nudging (LHN) scheme. Later the the convective capabilities of the COSMO-2 model are investigated through some case studies.

1.2 Recent applications of radar data in hydrological models

A hydro-meteorological flash flood forecasting system is generally based on the combination of three elements: a numerical weather prediction (NWP) model, that provides short-range quantitative precipitation forecasts; a remote sensing precipitation detection system, for storm monitoring and for the possible initialization and conditioning of the NWP model; and a hydrological hydraulic forecasting model, capable to forecast the stream response from the rain input (Norbiato [2008], Collier [2007]).

Short-range precipitation forecasts have until recent years mainly been based on extrapolation techniques, and indeed, work continues to improve such techniques (Li and Lai [2004]). Even though these approaches have shown some success (Berenguer et al. [2005]; Van Horne et al. [2006]), extrapolation techniques may fail to develop convection in new areas and to describe cell splitting and decay, which often control flash flood dynamics (Collier [2007]). The recent introduction of a new generation of NWP models capable to simulate, and potentially forecast, deep convection events explicitly offers the prospect of producing useful forecasts of convective storms on scales applicable to flood prediction. Deep convection is often associated with flash floods, given its capability to produce large rainfall accumulation in a short period of time. The concept of numerically predicting highly convec-

tive storms was proposed nearly two decades ago (Lilly [1990]; Droegemeier [1997]). More recent demonstrations of the utility of convective-scale numerical weather prediction (Xue and Droegemeier [2003]; Weisman et al. [2008], among others) and the continued rapid increase in affordable computational resources, suggest that numerical forecasts is becoming an important component of convective-scale warning operations. However, given the difficulties in describing accurately the relevant initial conditions, the expected benefits rely also upon appropriate data assimilation techniques which are consistent with the small spatial scales involved. Hereby, radar rainfall and Doppler wind assimilation plays a central role, in that weather radars provide quasi continuous observations of precipitation systems, both in time and space.

Early assessments of the potential of NWP quantitative precipitation forecasts (QPF) for flood forecasting were made during the Hydrological Radar Experiment (Moore et al. [2000]). A real-time discharge forecast exercise by coupling NWP and hydrological models was performed during the 70-day Special Observing Period of the Mesoscale Alpine Programme (MAP) (Bougeault et al. [2001], Benoit et al. [2003]). In COST 731 on Propagation of Uncertainty in Advanced Meteo-hydrological Forecast Systems (Rossa et al., submitted for publication) the coupling of meteorological and hydrological models is treated more systematically, giving particular attention to the estimation of flood event probabilities (Zappa et al. [2010]). Radar data assimilation methodologies are further explored in the context of cloud resolving models and deemed as a promising avenue to improve convective scale QPF(Rossa et al. [2011], and references therein). These recent developments in operational convection-permitting NWP allow to explore the potential of such systems to simulate and forecast extreme, flash flood producing convective precipitation events. Chancibault et al. [2006] reported on a full hydro-meteorological coupled system, which was shown to reproduce and forecast the essential hydrological details of an intense flash flood event occurred on 5–9 September 2005 in southerncentral France.

In this contribution are shown some preliminary experiments of coupling of a high resolution meteorological model with an Hydrological one.

Chapter 2

Data and methodology

2.1 The numerical model

The numerical model COSMO-2 is the operational MeteoSwiss implementation of the high-resolution version of the non-hydrostatic weather forecasting model of the COSMO (Consortium for small-scale modelling) community presently operational at several European Weather Services [Doms and Schättler, 2002, Steppeler et al., 2003]. The COSMO-2 model domain covers the Alpine arch (520 x 350 grid points, 60 vertical levels) and uses a horizontal mesh size of 2.2 km. The NWP system of MeteoSwiss, with the corresponding forecast domain at 7 km and 2.2 km is shown in fig: 2.1.

In the COSMO model the three-dimensional fully elastic and non-hydrostatic atmospheric equations are solved numerically with second or third order finite difference methods on a Arakawa- C/Lorenz grid based on a rotated geographical (lat/lon) coordinate system. No scale approximations are performed. Vertically a stretched terrain-following grid (Gal-Ghen and Sommerville [1975]) is used and an option for the SLEVE vertical grid is also available

Prognostic variables include pressure perturbation, three wind components, temperature, specific humidity and turbulent kinetic energy. In addition, precipitation processes are explicitly described using a bulk-type cloud microphysics scheme containing five prognostic hydrometeor types (rain, snow, cloud water, cloud ice and graupel).

The physics package of COSMO considers 6 main components: radiation, precipitation microphysics, convection, soil and surface processes, turbulence in the atmosphere and turbulent transport at the surface.

While shallow convection is parametrized, a parameterization for deep convection is not used. The COSMO-2 forecasts, covering the central Europe,

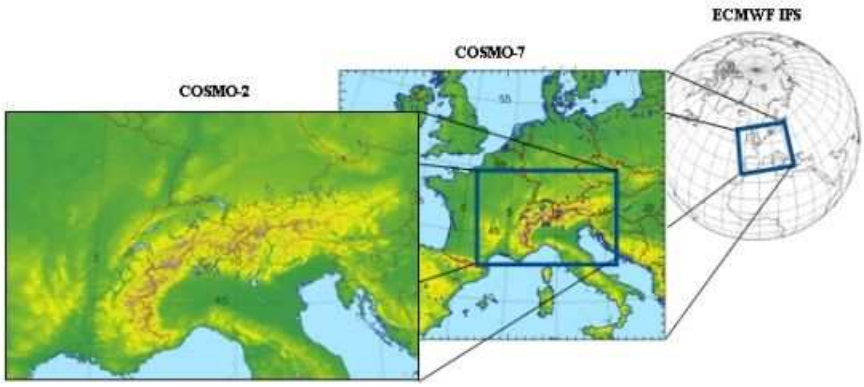

Figure 2.1: Setup of the MeteoSwiss NWP system based on the global model IFS for boundary conditions and initialisation of COSMO-7, COSMO-7 with 7 km horizontal resolution and COSMO-2 with 2.2 km resolution.

are driven by the regional COSMO-7 model with 6.6km mesh size, which in turn is nested in the global IFS model of ECMWF. The COSMO-2 model uses a data assimilation system based on a nudging technique (Schraff [1997]) for conventional observations from surface stations, radiosondes, aircrafts and wind profilers. Assimilation of radar data with Latent Heat Nudging technique is possible for high resolution simulations (e.g. 2.2. Km), revisited by Leuenberger and Rossa [2007].

Experiments performed with COSMO-2 concerned both assimilation than free forecacast mode. During an assimilation experiment the model, for each time step, incorporate observations of the current (and possibly past) state of a system with the results from the its calculation to produce an analysis, which is considered as 'the best' estimate of the current state of the system. This is called the analysis step. Essentially, the analysis step tries to balance the uncertainty in the data and in the forecast. The model is then advanced in time and its result becomes the forecast in the next analysis cycle. A free forecast experiment involves data assimilation only for a well defined period, 3 hours for example, then the model is free to calculate the state of the atmosphere for the remaining time of the experiment without any "help" from outside.

2.2 Data assimilation: LHN

Latent heat nudging (LHN) is a method which consists of forcing an NWP model towards observed precipitation rates. It is based on the observation that since relatively little moisture is stored in clouds, the column integrated

latent heating rate must be approximately proportional to the precipitation rate. The principle is to correct the model's latent heating at each timestep by an amount calculated from the difference between observed and model estimated precipitation.

This extra heating then acts as a source term in the thermodynamic equation, which in turn brings about an adjustment in the model vertical velocity field that brings the model precipitation rate closer to that observed.

LHN used in this assimilations closely follow Jones and Macpherson [1997], contributions to LHN are related to the parametrisation of precipitation used. The LHN scheme used in this work allows the prognostic treatment of precipitation as a variable and is advected in all three space dimensions. Stephan et al. [2008] proposed a modified LHN scheme to take into account the spatial and temporal separation of the rate of change in latent heating and surface precipitation and make the LHN algorithm more compatible with the prognostic precipitation scheme of the COSMO model. This improved LHN scheme is employed in operations in COSMO-2 and used in this study.

Single terms of LH equation for a level i of the model are explained in table 2.1:

$$LH_i = \frac{\Delta T_{LH}^{mod}}{\Delta t} = \frac{L_V}{c_{pd}}(S_c - S_{ev}) + \frac{L_S}{c_{pd}}(S_{dep} + \frac{L_F}{c_{pd}}(S_{nuc} + S_{rim} + S_{frz} - S_{melt}))$$

Symbol	Definition / Description
L_V	Latent heat (J/Kg) of vaporization
L_V	Latent heat (J/Kg) of sublimation
L_F	Latent heat (J/Kg) of fusion
c_{pd}	Specific heat (Kg K /J)of dry air at constant pressure
S_c	Mass transfer rate due (Kg/s) to condensation and evaporation of cloud water
S_{ev}	Mass transfer rate due(Kg/s) to the evaporation of rain in sub-cloud layer
S_{dep}	Mass transfer rate (Kg/s) due to the depositional growth of snow
S_{nuc}	Mass transfer rate (Kg/s) due to the formation of snow due to nucleation from cloud
S_{rim}	Mass transfer rate (Kg/s) due to the accretion of cloud water by snow (riming)
S_{frz}	Mass transfer rate (Kg/s) due to the hetereogeneous freezing of rain from snow
S_{melt}	Mass transfer rate (Kg/s) due to the melting of snow due to form rain

Table 2.1: Terms in the LH equation,

The LHN algorithm act on 3 steps:

1. Model physics and dynamic tendencies are derived from the current state of the model atmosphere.

2. The diabatic temperature tendencies related to phase changes of water for each grid point are calculated.

3. The LHN temperature increments ΔT_{LHN} for each grid points are calculated by scaling the profile by a factor related to the quality function if available (otherwise the scaling factor is equal to 1) and added to the prognostic temperature field at the end of each time step.

The LHN temperature increments ΔT_{LHN} added to the prognostic temperature field is calculated as follow:

$$\Delta T_{LHN} = (f - 1) \cdot \Delta T_{LH}^{mod}$$

Where the scaling factor $f = \frac{RR_{ana}}{RR_{mod}}$ is the ratio of analised and model rain rate,while $\Delta T_{LHN^{mod}}$ take into account the model LH tendencies.

In order to analyse rain rates, we consider a weighted sum of the radar-estimated and the model rain rate:

$$RR_{ana} = w(x, y) \cdot RR_{rad} - [(1 - w(x, y))] \cdot RR_{mod}$$

The observation weight $w = w(x, y) \in [0, 1]$ allows for a treatment of the radar quality.

For $w(x, y) = 1$ radar measurement are considered extremely reliable, so that the analysed rain rate is equal to the radar-estimated rain rate, while for $w(x, y) = 0$ the observations are rejected and the analysed rain rate is assumed to be equal to the model rain rate.

If there are large discrepancies between observed and modelled rain rates, the scaling factor f is limited by a factor α so that there is not too much heat added to or removed from the model. If at a grid point the observed rain rate is much larger than the model rain rate (this includes the case, where the model has no precipitation) no suitable profiles are provided by the model and a nearby grid point is searched within a given range, where the rain rate more closely matches the local observed rain rate. If such a point is found, the nearby profile is scaled. If no nearby point is found, an idealised Latent Heat profile, called climatological profile, is used for the scaling. In Table 2.2 the possible ranges for the ratio between observed and model rain rates and the corresponding scaling factor and profile are listed.

The LHN scheme allows an adjustment of the humidity in addition to the latent heating. This is accomplished by retaining the relative humidity during the LHN temperature adjustment. At gridpoints where a positive (negative) temperature increment is applied, this results in an increase (decrease) of the water vapour. At locations were $fgt1$ (i.e. where precipitation should

		scaling factor f	profile to scale
model fair	$1/\alpha_{down} \leq \frac{RR_{ana}}{RR_{mod}} \leq \alpha_{up}$	$\frac{RR_{ana}}{RR_{mod}}$	local profile
model too wet	$\frac{RR_{ana}}{RR_{mod}} \leq 1/\alpha_{down}$	$1/\alpha_{down}$	local profile
model too dry	$\frac{RR_{ana}}{RR_{mod}} \geq \alpha_{up}$	$\frac{RR_{ana}}{RR_{near/ideal}}$	nearby/local profile

Table 2.2: Ratios of observed and model rain rates and corresponding scaling factors and profiles.

be enhanced in the model), water vapor is additionally nudged towards saturation. A similar humidity adjustment was proposed by Manobianco et al. (1994).

2.3 The Veneto Radar network

Figure 2.2: Images of Mt. Grande radar

The Veneto Radar Network (VRN) consists of two EEC single polarization C-band Doppler radars, one located on Mt. Grande (near Teolo) a 470 m hill top 25 km southwest of the city of Padova , the other at sea level close to the border between Veneto and Friuli in northeast Italy (near Loncon). In

fig: 2.3 positions of the VRN. From August 2010 the Milano-Linate airport radar has been integrated in the VRN, it is a single polarization C-band Doppler radar located 7 Km away from Milan at 108 M amsl. The radar mesures are post processed by the Hydrometeorological Decision Support System (Conway et al. [2007]).

The key components of HDSS include:

- radar quality control including clutter removal, bright band identification, hybrid scans and scan filling.
- mosaicking of Veneto radar
- data processing through a suite of applications named Quantitative Precipitation Estimation and Segregation Using Multiple Sensors (QPE-SUMS) (Gourley et al. [2001])

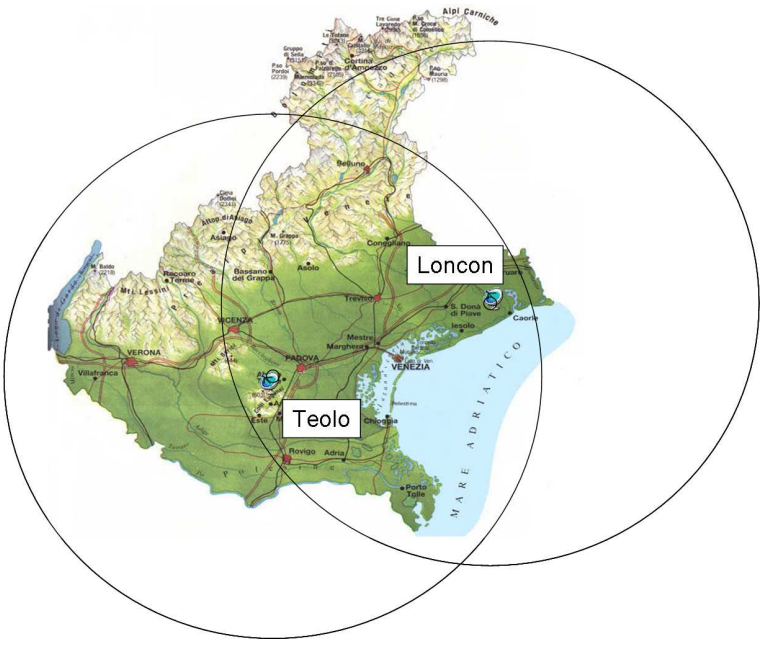

Figure 2.3: The veneto radar network(VRN)

Data and product outputs are available via customized web pages and a three-dimensional graphical workstation.

2.4 The Swiss Radar network

The Swiss Radar Network ([Joss, 1998, SRN]) consists of three C-band Doppler radars providing full volume information every five minutes. The

data are preprocessed and available on a Cartesian grid with a mesh size of $2 \times 2 \times 2\,km^2$ for the network composite.

The C-band radars Albis, La Dole and Lema are located on mountain tops at 925m, 1675m and 1625 m ASL, respectively. Fig 2.4 shows Swiss radars locations.

MeteoSwiss has more than forty years of experience with radar operation in mountainous region. Many efforts went into the optimization of hardware stability and data processing for the radar network.

Several studies regarded variations in the reflectivity-rainfall (Z-R) relationship and beam attenuation (Germann and Gabella [2004]).

At, MeteoSwiss, large efforts has been spent into producing RAIN, a two-dimensional map with the best surface QPE over Switzerland. This product has achieved from his birth a great improvement on quality, see Germann and Joss [2004a] for more details.

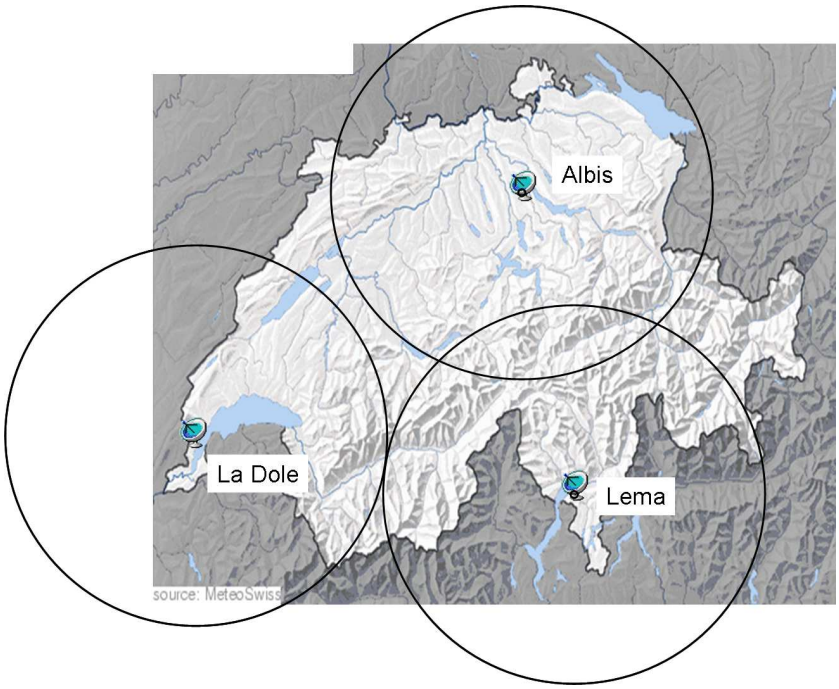

Figure 2.4: The swiss radar network(SRN)

2.5 Data set

Radar products, different for Veneto and Switzerland, has been treated through IDL (Interactive Data Language), a very powerful programming language for

analyzing and visualizing data. New routines has been created for Data analysis and to prepare grib files for radar data assimilation.

Table 2.3 provides an overlook on the main features of these data sets:

Table 2.3: Features of data sets

Case	Period	Time step	File type
Veneto	From 2005 to 2010	Every 15 minutes	NetCDF
Veneto	From 2010	Every 10 minutes	NetCDF
Swiss	From 2005	Every 5 minutes	Gif

Each Veneto NetCDF file contain various variables, like rain or snow preicipitation estimate for 1 and 3 hours and instantaneous rain rate, and various information pertaining to the radar domain. Swiss files used are very slim compared to Veneto and contain only instantaneaous estimated rain images that are interpreted and converted in precipitation values by some MeteoSwiss routines.

2.6 Verification methods

If we take the term forecast to mean a prediction of the future state, then forecast verification is the process of assessing the quality of a forecast. The forecast is compared, or verified, against a corresponding observation of what actually occurred, or some good estimate of the true outcome. The verification can be qualitative ("does it look right?") or quantitative ("how accurate was it?"). In either case it should give you information about the nature of the forecast errors. There are many types of forecasts, each of which calls for slightly different method of verification.

Forecast quality (the degree to which the forecast corresponds to what actually happened) is not the same as forecast value (the degree to which the forecast helps a decision maker to realize some incremental economic and/or other benefit). A forecast has high quality if it predicts the observed conditions well according to some objective or subjective criteria. It has value if it helps the user to make a better decision. Imagine a situation in which a high resolution numerical weather prediction model predicts the development of isolated thunderstorms in a particular region, and thunderstorms are observed in the region but not in the particular spots suggested by the model. According to most standard verification measures this forecast would

have poor quality, yet it might be very valuable to the forecaster in issuing a public weather forecast.

2.6.1 Standard verification methods

One of the oldest and best verification methods is the good old fashioned visual, or "eyeball", method: look at the forecast and observations side by side and use human judgment to discern the forecast errors. Common ways to present data are as time series and maps. However, the eyeball method is not quantitative, and it is very prone to individual, subjective biases of interpretation. Therefore it must be used with caution in any formal verification procedure.

A dichotomous forecast says, "yes, an event will happen", or "no, the event will not happen". Rain and fog prediction are common examples of yes/no forecasts. For some applications a threshold may be specified to separate "yes" and "no", for example, winds greater than 50 knots.

To verify this type of forecast we start with a contingency table that shows the frequency of "yes" and "no" forecasts and occurrences. The four combinations of forecasts (yes or no) and observations (yes or no), called the joint distribution, are:

- hit - event forecast to occur, and did occur
- miss - event forecast not to occur, but did occur
- false alarm - event forecast to occur, but did not occur
- correct negative - event forecast not to occur, and did not occur

The contingency table is a useful way to see what types of errors are being made. A perfect forecast system would produce only hits and correct negatives, and no misses or false alarms.

Categorical statistics used in this work are describeb below supposing a year's worth of official daily rain forecasts and observations producing a contingency table.

False alarm ratio (FAR)

$$FAR = \frac{false\,alarms}{hits + false\,alarms}$$

Answers the question: What fraction of the predicted "yes" events actually did not occur (i.e., were false alarms)?

Values: Perfect score: 0.

Characteristics: Sensitive to false alarms, but ignores misses. Very sensitive to the climatological frequency of the event. Should be used in conjunction with the probability of detection.

Probability of detection (POD)

$$POD = \frac{hits}{hits + misses}$$

Answers the question: What fraction of the observed "yes" events were correctly forecast?

Values: Perfect score: 100.

Characteristics: Sensitive to hits, but ignores false alarms. Very sensitive to the climatological frequency of the event. Good for rare events.Can be artificially improved by issuing more "yes" forecasts to increase the number of hits. Should be used in conjunction with the false alarm ratio (FAR). POD is also an important component of the Relative Operating Characteristic (ROC) used widely for probabilistic forecasts.

Probability of false detection (POFD)

$$POFD = \frac{false\,alarms}{correct\,negatives + false\,alarms}$$

Answers the question: What fraction of the observed "no" events were incorrectly forecast as "yes"?

Values: Perfect score: 0.

Characteristics: Sensitive to false alarms, but ignores misses. Can be artificially improved by issuing fewer "yes" forecasts to reduce the number of false alarms.

Threat score (TS)

$$TS = \frac{hits}{hits + misses + false\,alarms}$$

Answers the question: How well did the forecast "yes" events correspond to the observed "yes" events?

Values: 0 indicates no skill. Perfect score: 100.

Characteristics: Measures the fraction of observed and/or forecast events that were correctly predicted. It can be thought of as the accuracy when correct negatives have been removed from consideration, that is, TS is only concerned with forecasts that count. Sensitive to hits, penalizes both misses and false alarms.

Equitable threat score (ETS)

$$ETS = \frac{hits - hits_{random}}{hits + misses + false\ alarms + hits_{random}}$$

with $hits_{random} = \frac{(hits+misses)(hits+false\ alarms)}{totals}$

Answers the question: How well did the forecast "yes" events correspond to the observed "yes" events (accounting for hits due to chance)?

Values: 0 indicates no skill. Perfect score: 100.

Characteristics: Measures the fraction of observed and/or forecast events that were correctly predicted, adjusted for hits associated with random chance (for example, it is easier to correctly forecast rain occurrence in a wet climate than in a dry climate). The ETS is often used in the verification of rainfall in NWP models because its "equitability" allows scores to be compared more fairly across different regimes. Sensitive to hits. Because it penalises both misses and false alarms in the same way, it does not distinguish the source of forecast error.

True skill statistic (TSS)

It is a method for verifying multi-category forecasts and start with a contingency table showing the frequency of forecasts and observations in the various bins. It is analogous to a scatter plot for categories.

Answers the question: What was the accuracy of the forecast in predicting the correct category, relative to that of random chance?

Values: 0 indicates no skill. Perfect score: 1

Characteristics: Measures the fraction of correct forecasts after eliminating those forecasts which would be correct due purely to random chance.

2.6.2 Neighborhood (fuzzy) methods

High-resolution forecasts from numerical models can look quite realistic and provide the forecaster with very useful guidance. However, when verified using traditional metrics they often score quite poorly because of the difficulty of predicting an exact match to the observations at high resolution. 'Fuzzy' verification (Eberth [2008]) rewards closeness by relaxing the requirement for exact matches between forecasts and observations. The key to the fuzzy approach is the use of a spatial window or neighbourhood surrounding the forecast and/or observed points. The treatment of the data within the window may include averaging (upscaling), thresholding, or generation of a PDF, depending on the particular fuzzy method used and its implicit decision model concerning what makes a good forecast. The size of the neighbourhood can be varied to provide verification results at multiple scales, thus allowing the user to determine at which scales the forecast has useful skill.

Relative operating characteristic (ROC)

Plot hit rate (POD) vs false alarm rate (POFD), using a set of increasing probability thresholds (for example, 0.05, 0.15, 0.25, etc.) to make the yes/no decision. The area under the ROC curve is frequently used as a score.

Answers the question: What is the ability of the forecast to discriminate between events and non-events?

Values: 0.5 indicates no skill. Perfect score: 1

Characteristics: ROC measures the ability of the forecast to discriminate between two alternative outcomes, thus measuring resolution. It is not sensitive to bias in the forecast, so says nothing about reliability. ROC perfect curve travels from bottom left to top left of diagram, then across to top right of diagram. Diagonal line indicates no skill.

Fractions skill score (Roberts and Lean, 2008)

This approach directly compares the forecast and observed fractional coverage of grid-box events (rain exceeding a certain threshold, for example) in spatial windows of increasing size.

Answers the question: What are the spatial scales at which the forecast resembles the observations?

Values: 0 indicates complete mismatch. Perfect score: 1

Characteristics: This score is sensitive to rare events

Chapter 3

Construnction of an empirical radar data quality function

During the last few years interest in radar data quality has shown a shart increase due principally to the increase of quantitative use of radar observations in hydrology and the assimilation of these data in statistical framework as the variational assimilationv, that, however, rises issues not yet completely solved.

For operational uses we need a description of data quality in order to avoid assimilation of gross errors or zero values, where the radar is not able to work properly. The development od a radar data quality function represents a pragmatic approach to avoid investigation of the error covariance matrix (Keeler and Ellis [2000], Berenguer and Zawadzki [2008]).

3.1 Analysis of frequency of occurrence

Germann and Joss [2004b] show that a long-term precipitation accumulation calculated on more than 20-30 days has a direct correspondence with radar visibility, that is defined as the radar's ability to detect wave reflected by targets. From this starting point the empirical approach for producing this radar data quality function is that also the frequencies of occurence of rain events can contain information on radar visibility under right condition like long term accumulation and range attenuation of the radar beam. Laudanna Del Guerra [2010] produced a preliminary evaluation of an empirical radar data quality function. We will now summarise its construction before evaluating its impact in a more specific manner.

This kind of analysis is based on the assumption that frequencies became lower and lower when we move from good to sub-optimal visibility areas,

while totally shielded zones have frequencies near zero.

At the same time, pixels that belong to high percentiles of frequencies are most likely non rain echoes, these include ground clutter returns and spurious signal due to anomalous propagation of the radar beam. Ground clutter can be considered as one of the most important source of of non-rain echoes, most of which is eliminated by appropriate clutter filter. However in order to minimize eliminating real rain echoes, clutter filters leave, for instance, some $2-5\%$ of the non rain echoes in the data (Germann and Joss [2004b]). This residual clutter, called rest clutter, often manifest as a small scale, quasi-static, random signal with medium to high intensity

In Fig: 3.1 is possible to compare frequencies of occurence f for Veneto and Swiss radar networks. Sub-optimal visibility and clutter are clearly shown, that are the principal features related to quality of radar data. In fact, shielding the radar sites from nearby obstacles produces a cone with null or low visibility that is reflected in areas with very low frequencies of occurence of rain events. At the same time, areas with very high values of frequencies are relsated with non rain echoes The most relevant among these are, for Veneto radars, the one produced on South-East direction which is produced by Mount Venda and two more on W-S-W direction which are in turn produced by Mount Madonna. In the upper part of Veneto images is also visible the shieding produced by the alps on the radar beam. For Swiss radar network the main cones are related with La Dole instrument, the radar on the left part of the image, and are in S-W and N-E direction. Areas with lower visibility are related also to deep valleys and with range effects. All swiss radars are placed above from 900 m asl and this can bring to have lower visibility areas in presence of deep valleys. On images are visible two zones with lower f that is possible to identify with Grisons and Valais. These two deep valleys are sensibly lower than radar sites and happens that some precipitation event may be lost. Range effects are also clearly visible with frequencies and accumulation that constantly decrease going away from radars.

For a better comparison with long-term frequency of rain occurence, the percentage of frequencies of occurence is calculated. In this kind of plots (not shown) are still clearly visible range attenuation, cones, deep valleys and clutter.

3.2 Rest clutter identification

Rest clutter pixels can be defined as non-rain echoes not eliminated by clutter removal algorithm, which can be present on about 2-5% of pixels. Rossa and Leuenberger [2008] showed that, for assimilation in convective-permitting

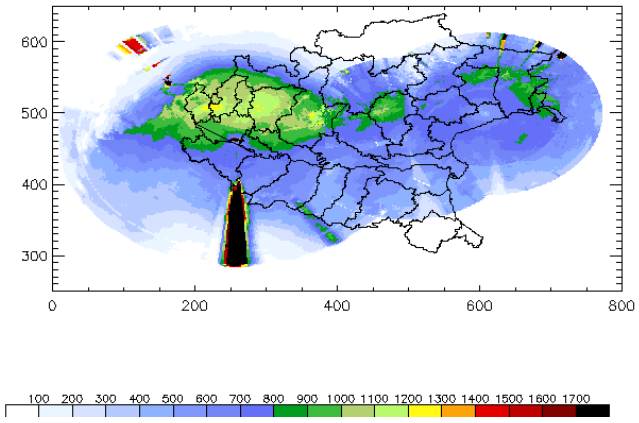

(a) Veneto frequencies

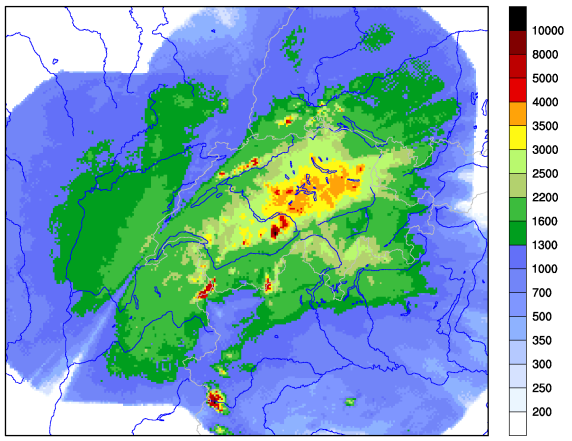

(b) Swiss frequencies

Figure 3.1: Frequencies of occurence of rain signal for VRN and SRN for a Summer (JJA) period. Pay attention to different frequency label between Veneto and Swiss (10 minutes vs 5).

NWP models, it is preferable to eliminate dubious non-rain echoes at the cost of underestimating rain events. Rest clutter is present in all accumulation images and is recognizable in isolated pixels with very high frequencies.The

main feature that identifies these pixels is their random signal which is not to be found in rainy ones. A rest clutter identification method, based on autocorrelation analysis, has been developed for this work. Lag correlation can be used for discriminate the different behaviour of rest clutter pixels from rainy ones thanks to the capacity of recognizing random signals. In fact, the lag correlation of the former decreases in a steeper way than the latter. If we produce time series of pixels over a period longer than 30 days, probable rest clutter pixels have demonstrated to have non zero signal in an absolutely random way. Rainy pixels, instead, have same periods with no signal alternate with consecutive time steps with signal detected.

Auto-correlation functions calculated for a sample population $X = \{x_0, x_1, .., x_{N-1}\}$ as a function of the lag (L) have this formulation:

$$P_x(L) = \frac{\sum_{k=0}^{N-L-1}(x_k - \bar{x})(x_{k+L} - \bar{x})}{\sum_{k=0}^{N-1}(x_k - \bar{x})^2}$$

Pixels with random behaviour have an auto-correlation that decreases in a steeper way than rain pixel as we can see on bottom left panel. Identification of rest clutter pixel is carried out by evaluation of a limit, $a'(0)_{min}$, on derivative of auto-correlation at $t = 0$. If $a'(0) = (\frac{da(t)}{dt})_{t=0} \leq a'(0)_{min}$ we identify this pixel as clutter. The $a'(0)_{min}$ limit has been chosen in empirical way through time series analisys of a great number of cases and has been set to -0.4.

Figure 3.2 show 4 time-series of QPE, autocorrelation and its derivative .We have 3 pixel with similar signal (nr. 1,2,4) which can be identified as rain while, the third, that has a different behaviour with something like noise superimposed to rain.

3.3 Quality function construction

The construction of a daily empirical radar data quality function here shown is based on long-term frequency of QPE occurence analisys and take into account:

- sub-optimal visibility areas
- clutter pixels
- range effects

The main idea is to categorize pixel quality as follows:

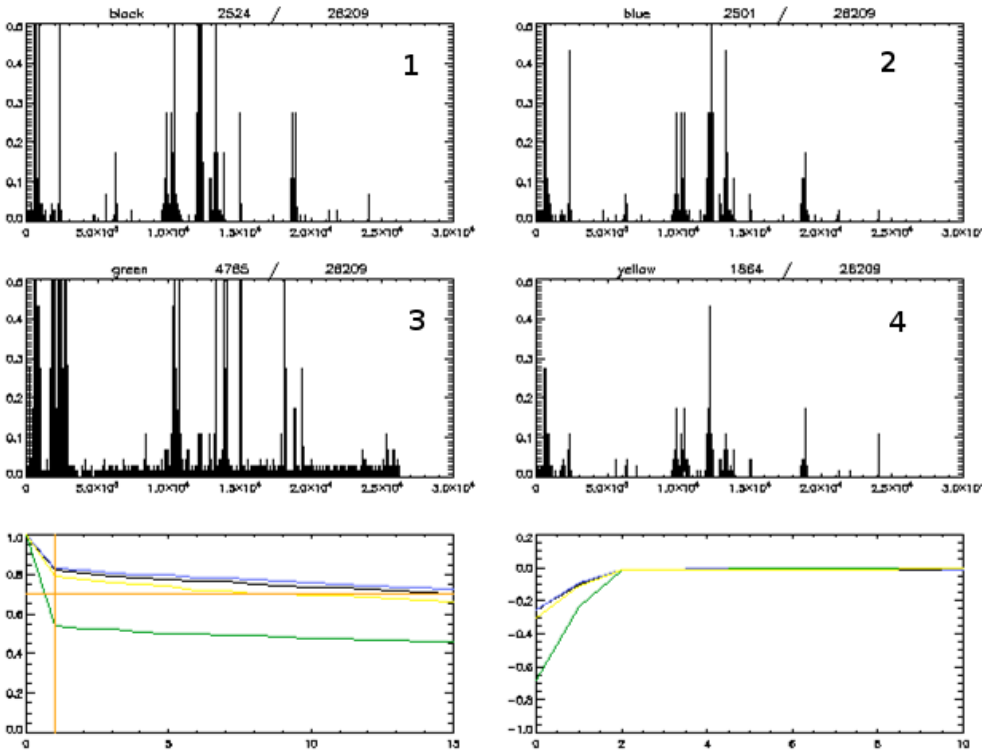

Figure 3.2: QPE time series for 4 VRN pixels, one probably clutter (nr. 3 and green curve),auto-correlations of them and derivative of auto-correlations.

- pixels which are seen too many times are likely to be rest clutter and are marked with a weight $w(x, y) = 0$ for frequency f greater than a threshold value fc;
- pixels which are regularly seen are likely to be of sufficient quality to be taken verbatim, i.e. $w(x, y) = 1$;
- pixels which are rarely seen, as for sub-optimal visibility areas, are likely to be in blocked areas and a weight decreasing from 1 to 0 with a function $g(f)$ is assigned to them starting from a frequency threshold f_0;

A conceptual definition of the radar data quality function is shown in fig:3.3 while the choice of the parametric terms is discussed in the discussion paragraph.

The procedure enacted to generate the daily radar data quality function is based on the analysis of a previous period, longer than 30 days, and can be summarized in 3 steps:

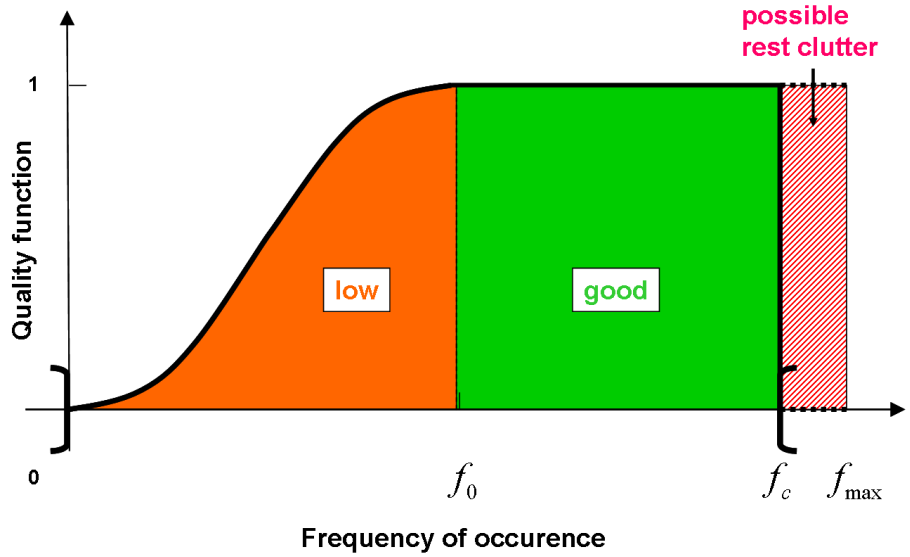

Figure 3.3: Conceptual definition of the radar data quality function.

1. loading the previous period pixel information of:
   - percentage of frequency of occurence
   - time series of higher frequencies pixels
2. updating all pixel informations by adding the next day and subtracting the first day of the series
3. Building a weighting function like this:

$$w(x,y) = \begin{cases} 0 & For\ rest\ clutter\ pixels \\ g(f) & For\ pixel\ under\ the\ value\ of\ f_0 \\ 1 & Elsewhere \end{cases}$$

3.4 Discussion

The choice of $g(f)$, f_0 and of the period of accumulation for the information to update are pivotal for quality function construction.

The $g(f)$ function has been chosen to smoothly reduce quality when considered sub-optimal, so that for instance range effects on radar beam can be represented in a smooth and plausible way. It should take care of range effects on radar beam, such as beam rising and its broadeningas well, with special care to transition between good pixel, with $w(x,y) = 1$, to pixel with

quality slightly worse. For this reason a function like:

$$g(f) = 1 - \frac{1}{1 + e^{(\frac{10 \cdot f}{7}) - 4}}$$

whith values that decrease slowly from 1 at the beginning, while, after, go down faster has shown the better performances. In fig: 3.3 the weighting function concept related with frequencies of occurrence is resumed.

The f_0 value can be seen as the border between good pixels and the ones affected by range effects; it has been evaluated empirically with a number of case studies and by comparison with the literature on range quality of radar data. The values adopted are 0.04 for the Veneto network and 0.07 for the Swiss network.it has been evaluated in empirical way through many tests compared with the literature on range quality of radar data.

The f_c, that is the threshold value over that the rest clutter identification algorithm is applied, has been chosen as the 0.92 percentiles because the great part of clutter is in this range and reducing the threshold requires too much calculationg capacity.

The other choice to be made for the construction of the weighting function regards the length of the accumulation period used as pixel information on step 1. In the perspective of updating such an analysis by adding the latest day while taking out the oldest in the data set, the length of the period should be long enough to avoid too large day-by-day variability, while it should be short enough to allow for at least seasonal differences.

One-month periods proved to be rather short, while three-month periods seem more adequate. In fact, for a thirty days period, 1 day is approximately 3%. If we add a no rainy day and subtract a day with a lot of signal we loose almost 6% of signal.

A careful consideration has bring to reckon the seasonal variability plausible in that in summer the precipitation systems reach higher altitudes than in winter so that they are seen at longer ranges. This fact yield better quality on the function in summer and is also true for some areas behind cones, in fact, higher precipitations systems can be seen by the radar above obstacles.

3.5 Results

Final results for the Veneto radar data quality function can be seen in fig. 3.4: Mount Venda and Mount Madonna cones (the two nearby hill peaks) are clearly outlined in weighting function $w(x, y)$, as are the shielded areas behind the prealpine chain to the north and the Appennines to the South. Is also possible to note the detection of rest clutter areas, the white areas on the

prealpine chain and the high frequencies cone presents in the Milano Linate radar, and the loss of quality due to range. Particularly Alpine areas, as Dolomites, are present in the Summer quality function while in the winter one these areas are not visible.

Results on the application at the Swiss Radar Network of the empirical quality function previously described are shown in figure 3.5. Here can be seen that the main and well known error prone areas are reproduced by the quality function, i.e. the cones due to nearby obstacles of the La Dole radar, the scarse visibility in the valleys like the Valais and the Engadin, the attenuation effect with range in all three radars, as well as a number of small scale rest clutter areas. A seasonal difference on long range quality it is also clearly visible, as for VRN quality function; particularly, the quality is reduced in winter. This feature is evident over the mountains to the north as in the La Dole radar cone extending to the northeast that is much more pronounced in winter than in summer. The rest clutter pixels, in figure areas with white color, are remarkably stable and tend to be larger in winter than in summer.

3.6 Impact of the radar quality function on data assimilation cycle

In order to asses the impact of the quality function with neighbourhood verification 2 periods of 13th days of assimilation were studied for the Swiss area. (tab. 3.6).

Radar Network	**Date**	**Exp. type**
Swiss	1-14/05/2009	Assimilation
Swiss	5-18/07/2009	Assimilation

Table 3.1: Case studies for the radar data quality function

Both 13-day periods werw characterized by both convective events and frontal passages, they has been chosen to evaluate the behaviour of the quality function on longer rain periods and not for some particularly event as has be done in Laudanna Del Guerra [2010].

The assimilation experiments on 13-day periods present (Fig. 3.6) artificially looking structures in the rainfall accumulations in the region of radar domain borders, in particular N-W corners appear to be significantly dryer than surrounding with a step from neighbouring areas that can reach 100mm,

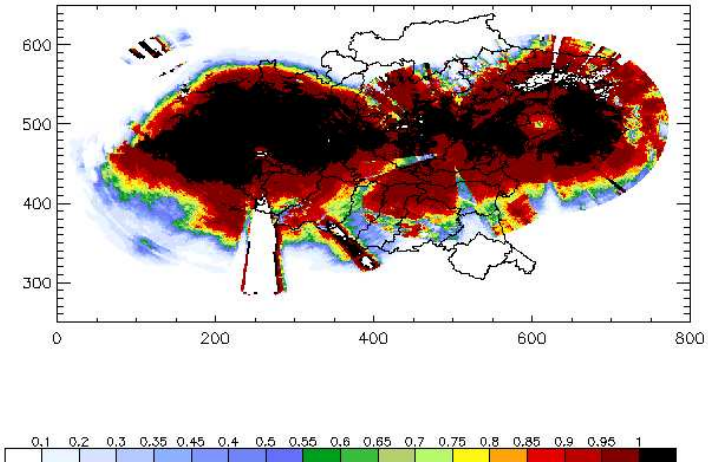

(a) Veneto DJF

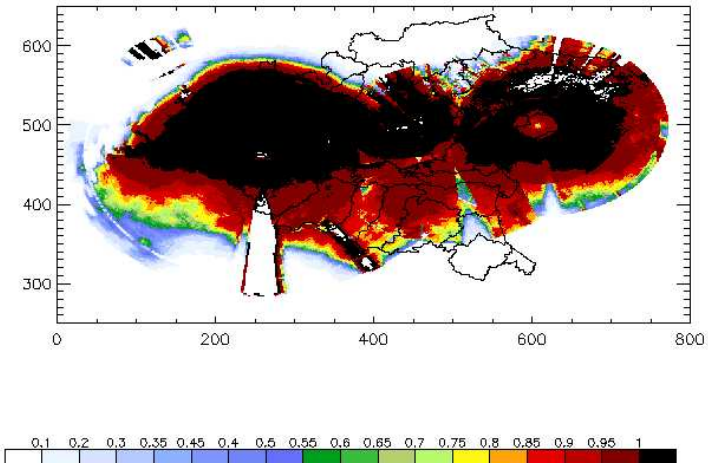

(b) Veneto JJA

Figure 3.4: Radar data quality function for VRN for winter and summer period.

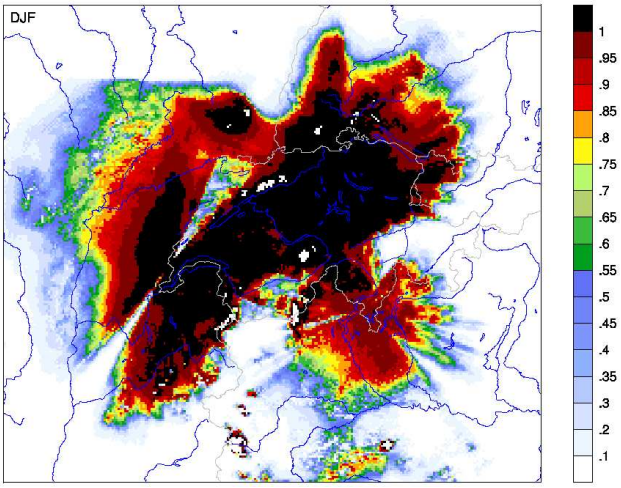

(a) Swiss DJF

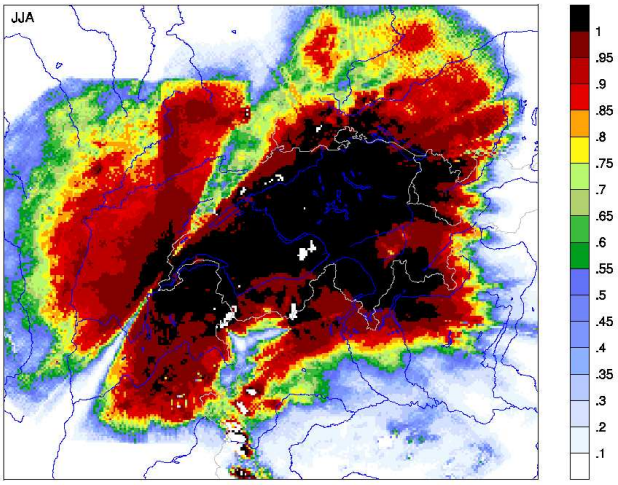

(b) Swiss JJA

Figure 3.5: Radar data quality function for SRN for winter and summer period.

these results are in agreement with the previous ones obtained for daily cases and with the conceptual model that give a possible explanation of this kind of artefact (Laudanna Del Guerra [2010]).

Introducing information on quality of radar data brings to a strong re-

duction of these artefacts and to a more continuous precipitation field, the differences are very significant, for example on the N-W corner the use of quality function avoid the removal up to 60-70 mm. Differences are largest in the region of the radar domain borders, but they stay large also in the interior of the domain. As all experiments overestimate the precipitation, the one with lowest is the best in terms of frequency bias, meaning that this is LHN without quality function. But this result is for the wrong reason as we know, since the reduction is mostly at the borders and in an "unhealthy" way, because it is due to a bad quality of radar information.

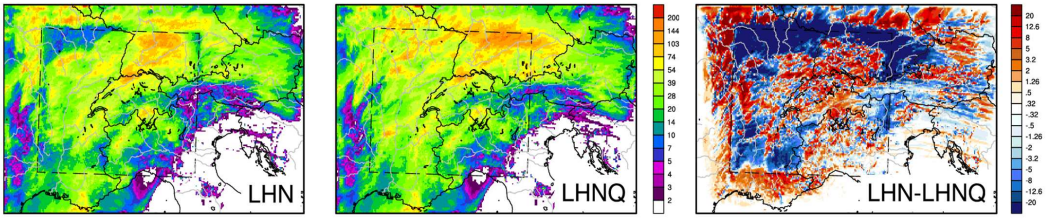

Figure 3.6: Rain quantitatives (mm) for the 1-14/05/2009 period on the swiss domain for assimilation with (LHNQ) and without (LHN) quality function, differences are represented in the third panel(LHN-LHNQ)

Verification with ETS and FSS differences shown that LHN with quality function slightly beats LHN without quality function, especially for low thresholds and over all scales(Fig. 3.7). This applies particularly for ETS.

From Fig. 3.7 is also possible to note that ETS differences are slightly positive also for small spatial scale this mean that the quality function, whose impact is especially large at the radar domain boundaries, has also a positive impact in the interior of the radar domain through downstream effects. Fuzzy verification with ROC method shown as, accounting for radar data quality, further improves the COSMO-2 precipitation slightly but constantly for all thresholds as can be seen in Fig. 3.8. Note, as well, the great favourable impact of LHN respect simple assimilation without radar data.

Other quantities, like 2mt temperatures, 10 mt winds and humidity don't show differences visible between the experiments. Overall, the experiments without radar data assimilation slightly worse in all scores and all variables.

3.7 Summary and conclusion

In this contribution an empirical quality description of radar derived QPE has been extensive evaluated. It is novel, yet simple, and based on long term

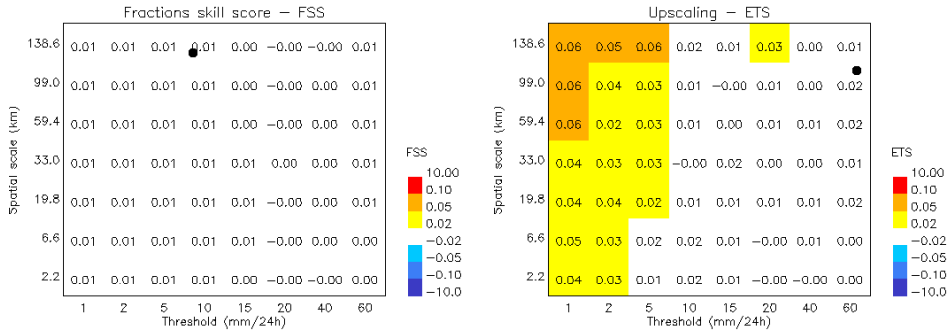

(a) (b)

(c) (d)

Figure 3.7: Impact of quality function over Switzerland. Neighbourhood verification score differences between LHNQ and LHN. a) shows ETS differences and b) fraction skill score differences. c) and d) are similar but fot LHN and NOLHN experiments

frequencies of occurrence of precipitation analysis. Hereby frequent (rare) occurrence of precipitation is assessed as 'good' ('bad') quality, while rest clutter was identified and assigned quality zero. Three suites of the convection permitting NWP model COSMO-2 were run for singles case studies and for extended periods. the setups were characterized through the use of radar QPE and of the proposed radar data quality function (Tab. XX). Evaluation was done by analysis of rain accumulation map and via statistical verification with neighbourhood methods. The empirical radar data quality function proposed with a moving 90-day accumulation window has the following characteristics:

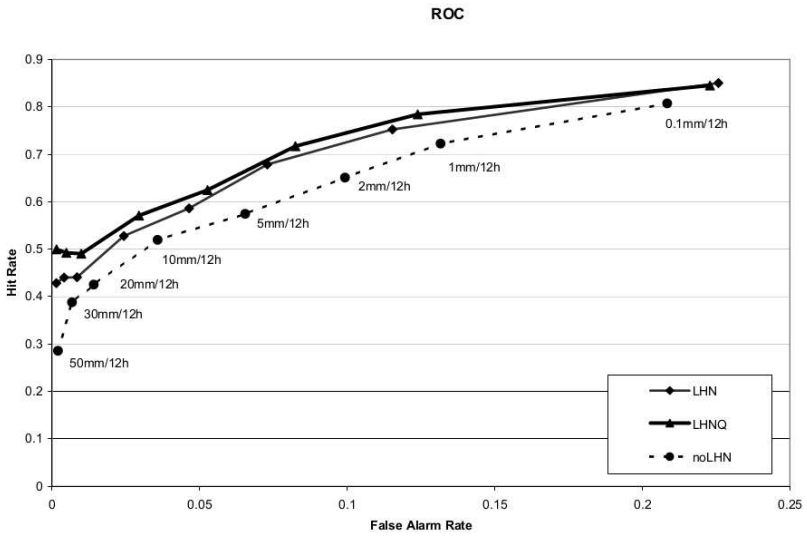

Figure 3.8: roc

- it is conceptually simple and easy to construct
- it reproduces the main error structures and is, therefore, a plausible way to account for the average problems in radar QPE
- it has a sufficiently smooth day-to-day evolution for an Alpine climate
- it accounts for the seasonal variability of the radar QPE
- it is, to some extent, generic, in that it can 'easily' be evaluated for different radar networks (here for two) and, potentially, also for heterogeneous networks in that it does not rely on specifics of the radar processing.

The beneficial impacts of this empirical quality function can be resumed in:

- Small but consistent improvement of COSMO-2 precipitation analyses
- Largest benefit at high thresholds and due to higher hit rate

- reduces artifacts which can be induced close to boundaries of the radar domain;
- constitutes an additional means to reduce rest clutter and its potentially harmful impact on the analysis
- does not artificially interfere with the model precipitation in areas where the radar is (almost) blind

While the limitations of such an empirical radar data quality description are recognized in that: empirical and not physically based

- average, not instantaneous
- good(bad) quality in caso of prec. higher(lower) than climatology
- the quality is described not in units of precipitations
- if a radar network miss for long period is a problem

This work has posed the basis for operational assimilation of quality function in meteoSwiss COSMO-2. Some obvious extensions to this work deals with the evaluation of the impact of quality function use for free forecast and of the function construction, particularly values of constants and accumulation periods lengths.

Chapter 4

Convective capabilities of the Latent Heat Nudging scheme for two extreme events.

In this chapter the convective capabilities of the COSMO-2 model are investigated through thha analysis of two case studies.

4.1 Case studies

In order to asses the impact of Latent Heat Nudging on extreme convective events some experiments were run for 2 case studies, both characterized by high precipitation amounts and intensitiy that caused flash foods with severe damages and loss of human lives. The first case study is the Mestre (VE) flash flood of the 26/09/2007, the latter is the events regarding the Fella river basin (UD) that happened the 29/08/2003.

4.1.1 Mestre flood

The 26 September 2007 storm was characterized by exceptional rain fall intensities (up to 120 mm, 90 mm, and 24 mm for the 1 h, 30 min, and 5 min maximum accumulations, respectively, all recorded at the Marghera raingauge station), and overall accumulation (320 mm for the 6 h maximum) as can be seen in Fig. 4.1. These were the largest precipitation events recorded in this area since 1956. Return periods, estimated by means of the methodology reported in Norbiato et al. [2007], were in excess of 400 years. The storm caused severe flooding over the urbanized area of Venice-Mestre and was produced by a long-lasting, quasi-stationary Mesoscale Convective

System (MCS, e.g. Weisman and Klemp [1982]; Schiesser et al. [1995]).

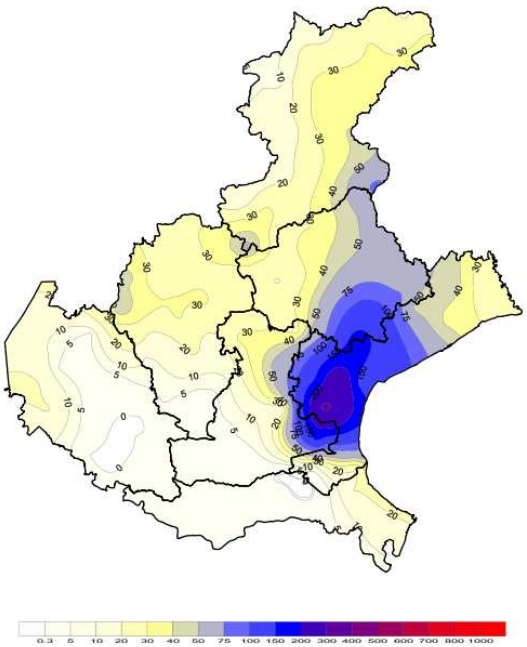

Figure 4.1: Veneto rain gauges accumulation of 26 september

The synoptic situation at 00 UTC was dominated by an upper-level trough over France which elongated into the western Mediterranean and a surface low developing in the Gulf of Genoa (Fig. 4.2 a) taken from the ECMWF analysis valid at 26 September 2007 00 UTC). The associated cold front was still over the western Mediterranean at this stage, while the Po Valley, and the Adriatic coast in particular, were in the south-easterly warm sector flow. Over the next twelve hours the front propagated eastward and occluded over the Po Valley. The surface low extended eastward but its core remained over the Gulf of Genoa. The surface pressure at Venice dropped from 1010 hPa to 1003 hPa over the 24 hours of 26 September with an intermediate rise of 2 hPa in the hours affected by the thunderstorms, i.e. between about 07 and 13 UTC. The divergent upper-level south-westerly flow associated with the leading edge of the trough remained over the area of interest during most of the 26th.

At 00 UTC the surface winds over the Veneto plain were north-easterly and probably partially blocked by the Alpine range (Monai et al. [2006], Davolio et al. [2009]). By 02 UTC a south-easterly flow of more than 5 m/s established on the southern Veneto coast. By 05 UTC both the north-easterly and south-easterly flows intensified, while the latter was extending

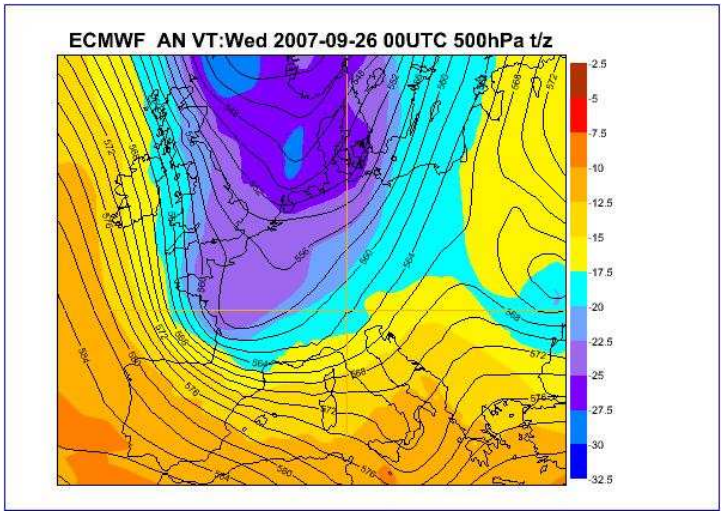

(a)

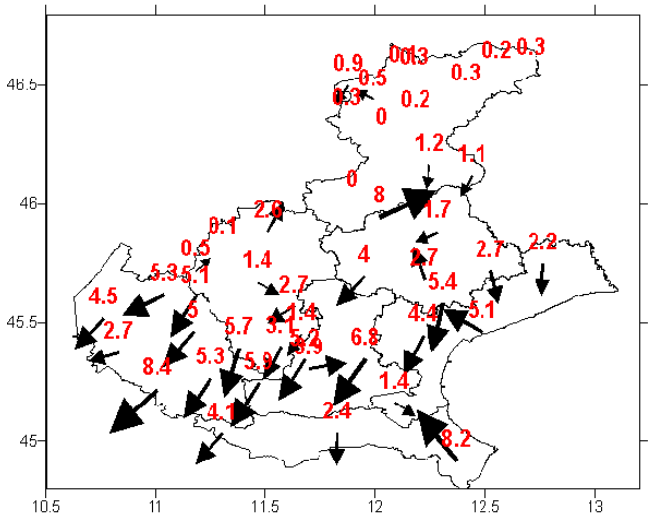

(b)

Figure 4.2: Aspects of the atmospheric flow configuration of the 26 September 2007 case: (a) upper-level flow in terms of temperature (°C) and geopotential height (dam); (b) 10 m winds taken from the ARPAV automatic weather station network valid at 05 UTC (numbers denote wind speed in m/s).

northward (Fig. 4 b) being also recorded at the station of Venice Cavallino. The resulting convergence was sustained until at least 07 UTC over the larger Venice area and propagated only slowly eastward onto the Adriatic thereafter.

As the convergence started and increased, the first cells developed some 20 km west of Mestre. These were followed by an intense, but low-topped, convective cell exhibiting an echo top between 6 and 7 km and a clear weak echo region. Interaction of the outflow of this cell with the mesoscale low-level winds triggered a second low-topped thunderstorm about one hour later which lasted until about 03:20 UTC. Both thunderstorm cells were indicative for significant convective instability. They were associated with high precipitation rates, but confined west of the area of flooding. Towards 04:00 UTC multicellular convection formed in the area of convergence diagnosed in the surface wind field. Note that at this point low-level warm and humid Adriatic air began feeding directly into the system from the east to form a mesoscale convective system. The flow configuration at this stage was such that the continuous regeneration of convective cells took place in the relatively circumscribed area of some 20 x 40 km^2 around and west of Venice Mestre. The MCS became quasi-stationary for about 4 hours, during which the exceptionally high rainfall rates and accumulations were recorded. After about 08:00 UTC the MCS propagated slowly eastwards and by 10:00 UTC the main activity was over the Adriatic sea. Accordingly, the rain over the area of interest started to decrease after 08:00 UTC and stopped after midday. Note that the MCS still exhibited significant rain intensities throughout the afternoon, but being located over the sea, they did not add to the hydrological emergency. For the sake of describing and evaluating the assimilation and forecast experiments it is useful to subdivide the case in three phases, i.e.:

- 01 - 04 UTC pre-MCS phase: scattered convective activity, including occurrence of intense convective cells, generally moving northwards; area averaged rainfall accumulation for this phase was 14.5 and 10.0 mm for the Mestre and Treviso area, respectively, local peaks reached 70 and 43 mm;

- 04 - 09 UTC MCS phase: beginning of organization of convective activity in a north-south oriented line just west of the area of interest at 04 UTC with subsequent intensification, meridional extension and slow eastward propagation onto the area of interest; most intense, flood-producing phase between 05 and 08 UTC; area averaged rainfall accumulation for this phase was 59.5 and 36.3 mm for the Mestre and Treviso area, respectively, local peaks reached 391 and 166 mm;

- 09 - 24 UTC post-MCS phase: further slow eastward propagation of line of convective activity onto the Adriatic with residual moderate convective activity over the area of interest; passage of widespread precipitation with some embedded convection during the evening hours; area averaged rainfall accumulation for this phase was 13.0 and 20.0 mm for the Mestre and Treviso area, respectively, local peaks reached 97 and 74 mm.

4.1.2 Fella flood

On 29 August 2003, at the end of a prolonged drought, a mesoscale convective system affected the area of the Fella basin (UD), starting at 10:00 local standard time (LST) and lasting for approximately 12 h. Accumulated precipitation measured up to $88\,mm/1\,h$, $233\,mm/6\,h$ and up to $400\,mm$ for the total event. A surface low located between the Spain and the gulf of Biscay was pushed by some Arctic air towards East and the Alps, Its interaction with a warm anticyclone located on the center of the Mediterranean sea, brought to very strong winds, from S-W in altitude and from S at the surface. This air was very humidy and warm due to an extremely warm summer.

A noticeable characteristic of the precipitation event was its organization in well-defined band structures. The steadiness of these rainbands led to highly variable precipitation accumulations.The storm total rainfall distribution reflects the southwest–northeast motion of the storm elements and west–east shift of the tracks of the storms and can be distinguished into three phases:

- An initial period (0800–1100 UTC), with the rainfall maxima (60–70 mm), extended over an elongated region at the western periphery of the Tagliamento, close to the Veneto–Friuli border.

- In the second period (1100–1700 UTC) an explosive growth of precipitation can be recognized over the right-hand tributaries of the Fella River system, associated with orographic enhancement. A maximum of 350 mm is identified over the region comprised between Pontebbana and Uqua.

- In the last phase (1700–2000 LST) the precipitation accumulation splits in three regions, with maximum of precipitation still concentrated over the Aupa and a less organized precipitation insisting over the Slizza River system, at the eastern border of the Tagliamento River basin.

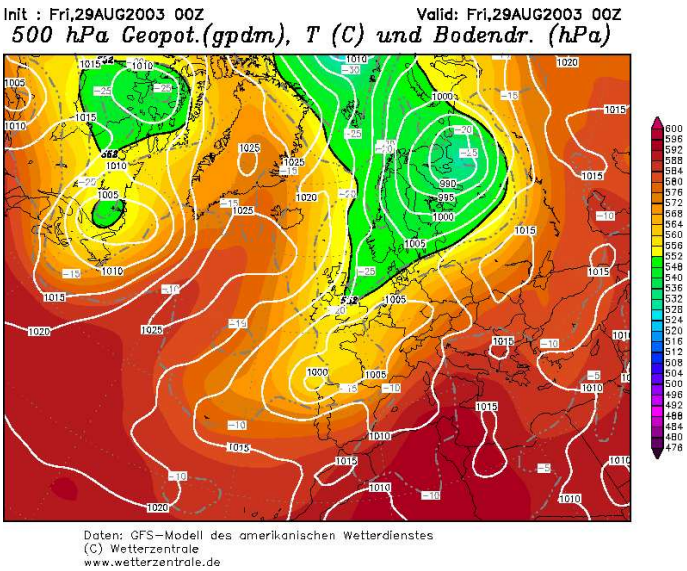

(a)

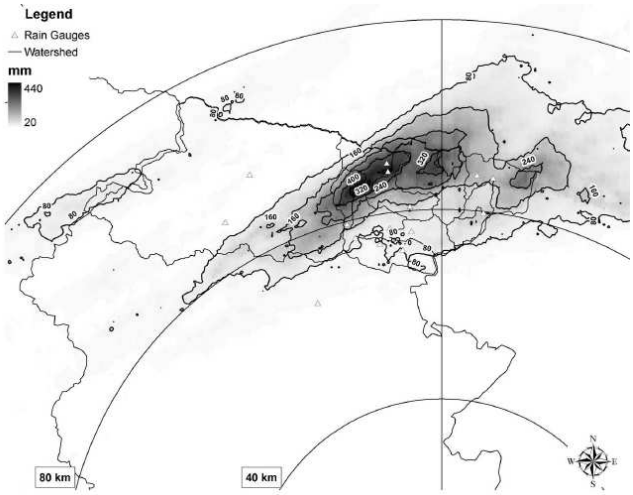

(b)

Figure 4.3: (a) upper-level flow in terms of temperature (°C) and geopotential height (dam) taken from the ECMWF analysis valid at 29 August 2003 00 UTC; (b) Fella basins rain gauges accumulation of 29 of August

Prior to the development of convection, the atmosphere was characterized by strong instability as evidenced by the very high CAPE value on the Udine radio sounding of 29 August 2003 at 0700 LST (about 4000 J/Kg for the CAPE computed based on the most unstable parcel). Precipitable water computed for this radio sounding amounts to 44 mm and shows that the humidity content of the atmosphere was already high. The storm affected a 1500-km^2 area, and caused loss of lives and substantial disruption of the local economy, with damages close to 1 billion euro.(Tropeano and Sanna [2004])

4.2 Impact of the Latent heat nudging scheme

A range of experiments, described in table 4.2, have been carried out at the CSCS (Swiss national supercomputing center, Buin) on Cray XT4. They can be split into assimilations and forecasts. Assimilation experiments are useful to investigate if the model, driven all the time by correct informations, is able to represent the event, while free forecast experiments are performed to study the operational use of a numerical model.

experiment	**description**
REF	Assimilation of data without LHN for the whole period
REF_R	Assimilation of data with LHN for the whole period
FCXX	Assimilation till XX UTC then free forecast mode

Table 4.1: Experiments for the assessment of the impact of the LHN scheme.

4.2.1 Mestre case

The reference assimilation simulation REF (Fig. 4.4 panel a)) was done without radar rainfall measurements and accounts only for sparse observations on the atmospheric state at the mesoscale over the Veneto region. The analysis cycle produces convective activity in and around the area of interest, but with a localization error of some 20-40 km, a timing error of 3-4 hours, while the simulated area-averaged peak rainfall intensity reaches about the level of the observed radar rainfall (Fig. 4.5 panel a) and b)). In more detail, first convective activity started after 03 UTC and by 05 UTC the convection had about the observed intensity and was located within 20 km of the area of interest. However, this cell then decayed moving north-eastward, while two new intense cells developed some 60 km west of Venice, one of which further

intensified and moved over the area of interest over the period from 08 to 18 UTC and became locked over the Lagoon starting 11 UTC. It produced significant rainfall throughout the afternoon with an hourly accumulation maximum of 65 mmh-1. After 18 UTC the precipitation lost intensity but remained coherent and propagated to the northeast and decayed over the Adriatic Sea.

Assimilation of the radar observation through latent heat nudging (LHN) improves the analysis dramatically, especially in terms of timing and localization. The main impact of the radar rainfall data on the assimilation cycle (REF_R) can be appreciated throughout the three phases of the event and may be summarized as follows:

- pre-MCS phase: the first cells are inserted in very good agreement with the observations between 01 and 03 UTC when no convective activity was present in the reference simulation; intensity of the simulated rainfall is about equal to the observed (Fig. 6 a); the incorrect cells of the reference simulation are suppressed, while the observed cells are correctly triggered at the right location;

- MCS phase: between 04 and 07 UTC the main MCS is triggered and kept in the correct location, however with significantly smaller intensity, while the main coherent convective system over the lagoon present in the reference simulation is suppressed for its entire life cycle, i.e. until 23 UTC;

- post-MCS phase: line of convective activity over the Adriatic successfully assimilated with slightly larger positioning errors.

Comparison of the REF_R experiment with the observed hourly radar accumulations reveals that the model precipitation fields are smoother and generally more extended in space (not shown). The structure of the main MCS in REF_R was, as mentioned, simulated very well, with only a slight positioning error of initially about 10 km west, growing to about 20 km by the end of the MCS phase. Also, the rainfall associated to a storm in the REF experiment which developed some 50 km west of the area of interest was correctly reduced by the LHN to the observed moderate values around 20 mm in six hours. The observed peak accumulation of locally 290 mm in six hours, however, are not reproduced in the assimilation experiment which yielded about 140 mm. This pinpoints the major limitation of this simulation experiment. Table 4.2 reports some key quantities which summarize timing and local peak rainfall associated with the main MCS in the various simulation experiments. Figure 4.5, on the other hand, shows the area-averaged

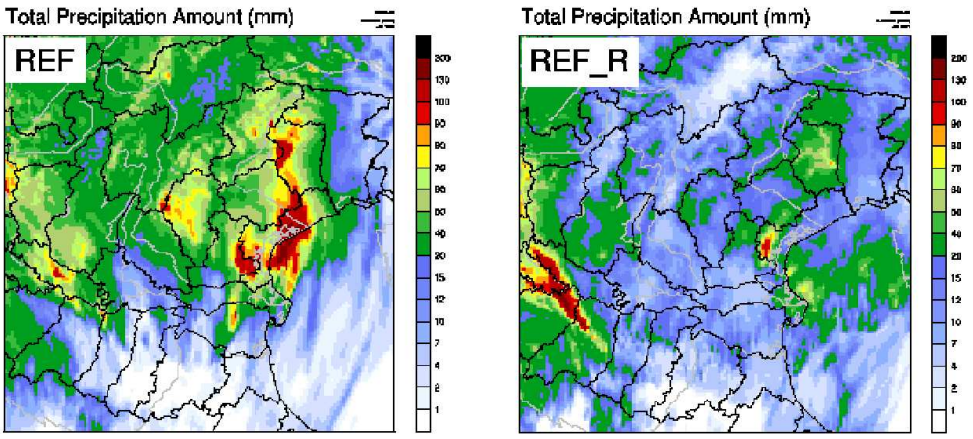

(a) REF

(b) REF_R

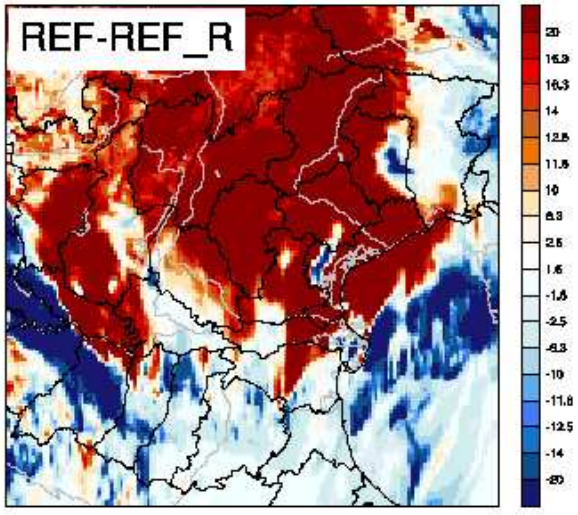

(c) RADAR

Figure 4.4: 24h accumulation of the Veneto case for REF, REF_R experiments and REF-REF_R differences.

hourly precipitation accumulations, for which the quantitative comparison give better results. In fact, for the area-averaged rainfall of the larger Mestre region, the REF_R reaches a peak of about 80% of the radar observations and shows about one hour of lag in the beginning of the event (4.5 a). This

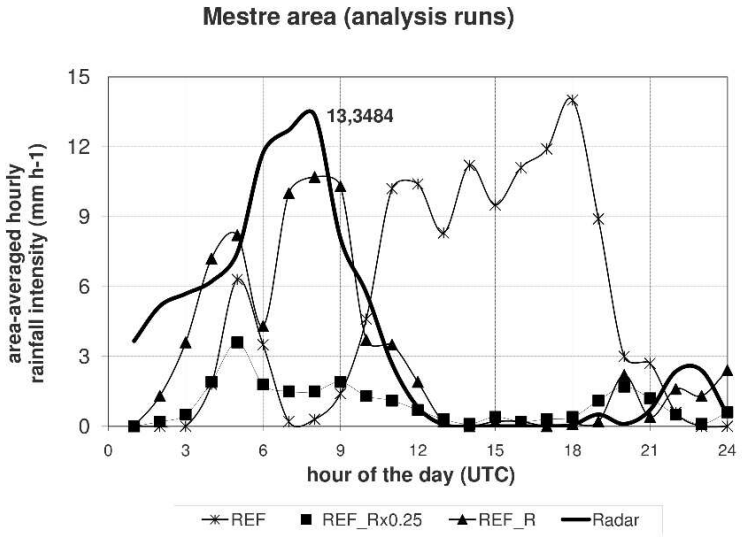

(a)

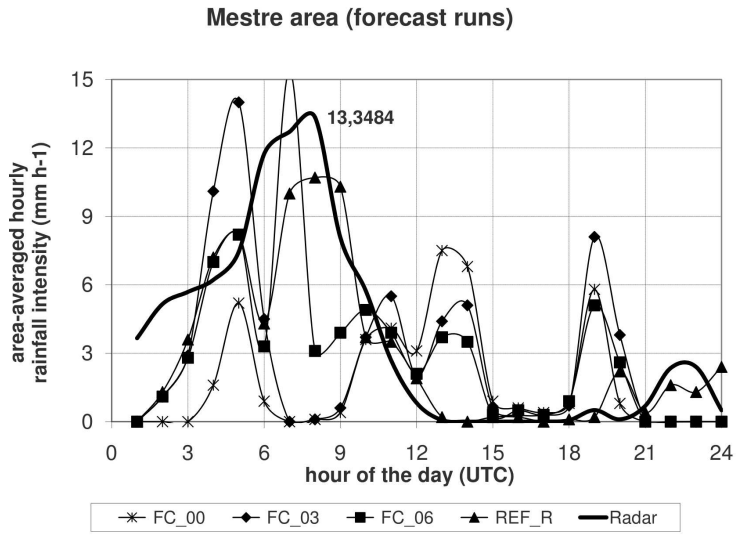

(b)

Figure 4.5: Time series of area-averaged hourly precipitation intensity (mm/h) derived from radar and simulations defined in tab. 4.2 for the target area of Mestre: a) represent assimilation experiments and b) forecast ones.

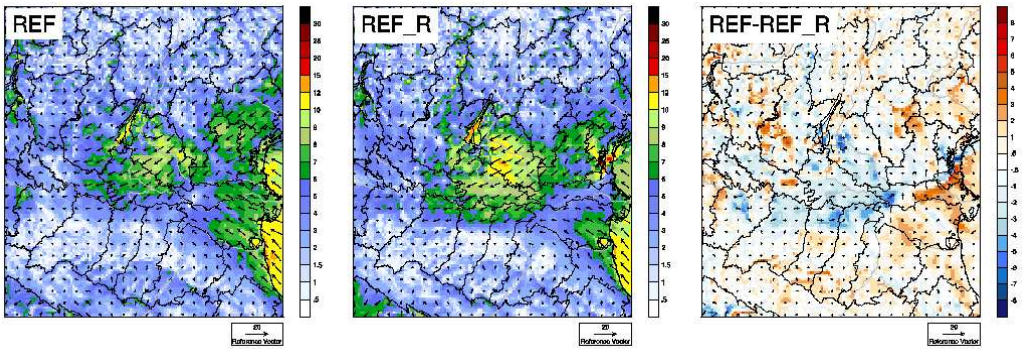

Figure 4.6: 06UTC wind direction and strength at the model lowest level for REF and REF_R experiments, the third panel represent REF-REF_R difference.

time lag may be explained by a systematic lag of the LHN scheme of in order of half an hour in triggering a convective cell (Leuenberger and Rossa [2007]). Figure 4.6 shows the low-level wind response of the model to the radar rainfall assimilation valid at 06 UTC. The low-level flow associated with the MCS is well developed during this mature stage and the magnitude of up to 8 ms-1 over the Po Delta compares well with the observations (Fig. 4.2 panel b). The distribution of the inflow into the main cores of the MCS, however, seems to have a more north-easterly component rather than the south-easterly component suggested by the observations on the coast. Also, the intensity of the model winds, which are indirectly forced by the LHN, are significantly higher than the measurements. In fact, the model flow in REF_R features the meridional flow component which turns to north-easterly off shore in the southern portion of the Venice Lagoon. The LHN continues to force vertical motion, and therefore horizontal inflow, until the simulated rainfall matches the observed. The fact that the inflow into the MCS is overestimated is therefore consistent with the underestimation of the model precipitation and indicates that too little moisture is fed into the updraft.

During the post-MCS phase the organized convection over the Adriatic Sea is simulated with similar positioning discrepancies of the order 10 to 20 km. The widespread precipitation observed during the evening hours are reproduced. As mentioned above, and clearly put on display in (Fig. 4.4), the rainfall assimilation manages to suppress the intense and stationary convection in the REF experiment for its entire life cycle. For the Treviso area the quantitative comparison gives even better results. REF_R reaches over 110%, in some hours more, of what was recorded by the radar. The simulated rainfall does, however, decrease two hours too early in the post-

Experiment	QP max	timing (UTC)	$\sum 6h(mm)$	$\sum 24h(mm)$
RADAR	159.0	07:00	328.0	410.0
REF	28.0(65.0)	05:00 (15:00)	32.0	140.0
REF_R	41.0	06:00	108.0	265.0
FC00	19.0(36.0)	05:00 (20:00)	19.0	90.0
FC03	43.0(37.0)	05:00 (20:00)	65.0	101.0
FC06	32.0 (25.0)	04:00 (19:00)	72.0	137.0

Table 4.2: Precipitation local peak accumulation for 26 September 2007: key figures of radar QPE, assimilation and forecast experiments in terms of hourly, 6- and 24-h accumulations and the corresponding timing. Values in bracket for QP max and timing indicate the evening peak in the simulations which was not actually observed.

MCS phase. In the pre-MCS phase the convective activity in the assimilation run REF_R is initially underestimated but reaches reasonable values by 03 UTC.

Free forecast runs were conducted starting from the analysis of 26 September 2007 00 UTC (FC_00), i.e. from the REF simulation at that hour, from 03 UTC (FC_03) and 06 UTC (FC_06) of the REF_R analysis containing the radar rainfall information starting from 00 UTC and then compared to the reference analysis simulation REF_R (see Tab. 4.2). FC_00 has a similar overall structure as REF with the two rainfall passages induced by upper-level disturbances that crossed the region around 13 UTC and the second after 20 UTC. However, precipitation in the free forecast is much weaker and does not produce the intense convection locked over the Venice Lagoon for several hours present in REF. Structure and intensity, on the other hand, were rather similar for the evening rainfall event. Overall, the maximum hourly rainfall intensities during the flooding event did not exceed 19 mmh-1 and would probably not have triggered a flood alert. This behaviour is well reflected in the time series of the area- averaged hourly precipitation shown in Fig. 4.5 c) and d), especially for the Mestre area. In the Treviso area the rainfall peak observed at 05 UTC is forecast with correct timing and an amplitude that reaches a bit more than 40% of the values observed by the radar. It does, however, fall off too quickly due to the missing MCS, while the incorrect afternoon and evening peaks are present in this area, too.

The free forecast FC_03 starts from initial conditions which contain the intense convective cell thunderstorm approaching its mature stage just west of the area of interest. The subsequent development of this cell is realistic, yielding about 150% of the hourly area-averaged precipitation observed

by the radar in both areae. In this simulation the circulation associated with the this cell does not interact with the convergent flow just inlands of the Lagoon to support the initiation of the MCS over the area of interest. Convection forms later over Mestre and surroundings in this simulation but not with intensities comparable to the observations. The overall benefit of the radar rainfall assimilation is two to three hours and corresponds to the lifetime of the intense cell present in the initial conditions, as well as the correct reduction of the wrong peak simulated at 13 UTC by almost 50%, i.e. some 10 hours into the free forecast. In the post-MCS phase the differences between the FC_03 and the FC_00 experiments are in the details of the evolution of the convective rainfall, but by 20 UTC the two simulations are practically identical. The FC_06 forecast starts from initial conditions which contain the main MCS in an already developed stage. As a result convection is kept in the subsequent free forecast over the area of interest for about five hours. Also the wrong peak simulated at 13 UTC is correctly reduced in this simulation by almost 60% for the Mestre area and more pronounced for the Treviso area, i.e. some 7 hours into the free forecast. The area-averaged hourly rainfall is in good agreement with the radar observations for 07 UTC, after which however the convective development suddenly weakens to significantly weaker intensity, and the smoother and broader structure. Again, the local peak values compare less favourably, and for the afternoon and evening hours similar precipitation patterns are simulated as in the FC_00 and FC_03 experiments.

4.2.2 Sensitivity analisys

A number of sensitivity experiments were performed with respect to the radar rainfall amplitude by scaling it with factors ranging from 1/8, 1/4, 1/2, 1, 1.5, and 2. This was done for two reasons, one being to assess the impact of radar amplitude errors on the LHN analysis, the other to investigate the model's capability to reproduce the extraordinary rainfall intensities. The LHN scheme is designed to force the model to reach the observed rainfall quantity, but due to its indirect forcing through heating and cooling, the model response takes some time. For quickly changing precipitation systems it can, therefore, be difficult for the model to attain a steady state (Leuenberger and Rossa [2007]). The main structures of the pre-MCS and MCS phase are reproduced quite similarly in all sensitivity experiments with intensities which are generally in line with the rainfall forcing. Figure 4.7 show the normalized areally averaged simulated precipitation for selected hours of the pre-MCS, the MCS, and the post-MCS phase, where normalization is relative to the area-averaged radar rainfall for this hour. This representa-

tion allows to appreciate to what extent the model response is proportional to the LHN forcing independently of the rainfall intensity. The dashed line corresponds to perfect linearity, i.e. what is forced is exactly reproduced by the model. For the Mestre area, the model response to the LHN is not producing the rainfall with which it was forced for QPE factor ≥ 1.0, i.e. it seems difficult for the model to produce very high rainfall rates. For the pre-MCS hours, here represented by 03 UTC, the response is quite linear. In the MCS hours, however, this linearity is no longer systematically fulfilled. For instance, for hour 05 UTC REF_Rx0.25 produces more rainfall than REF_Rx0.5 which was forced with twice the rainfall, while for hour 07 UTC REF_Rx2 produces 25% less rainfall than REF_Rx1.5 and about the same amount as REF_R. At the intermediate time 06 UTC the model response returns to be approximately linear with the rainfall forcing.

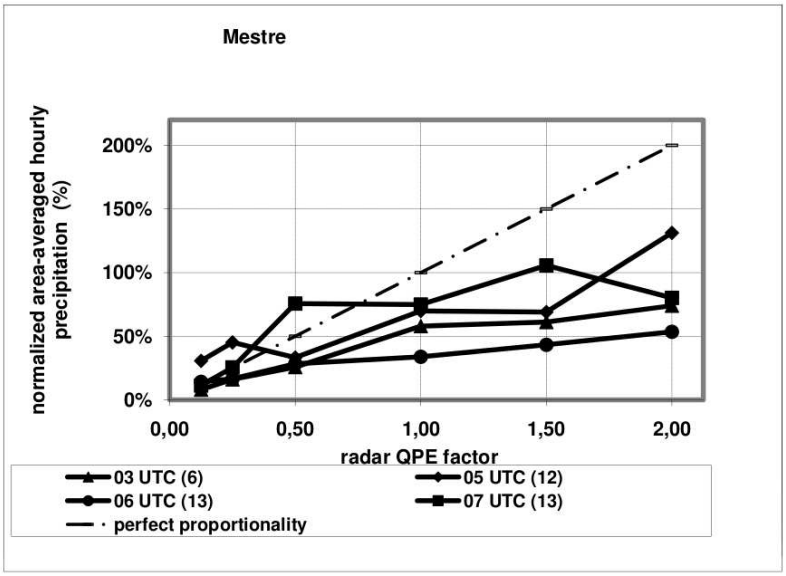

Figure 4.7: Normalized area-averaged hourly simulated precipitation (% of radar QPE) as function of the radar QPE scaling factor used for the sensitivity experiments.

The hours of strong non-linear model response correspond to the mature, very intense stages of the main convective systems for the hours with only

residual convective activity. The sensitivity experiments therefore indicate that QPE errors are propagated linearly into the atmospheric model state for moderate rainfall, in a less obvious and potentially non-linear way for intense to very intense rain, which is indicative for the fact that the model convective dynamics interfere with the LHN forcing. It is very difficult to attribute the cause for this behaviour, but it is likely that the very strong convective forcing induced by the LHN of can lead to flow interference in highly non-linear systems such as thunderstorms. Inconsistencies of the model versus real convective environment may add to these discrepancies (Leuenberger and Rossa [2007]).

4.2.3 Fella case

The choice of this case has been driven by the necessity to see the impact of the LHN scheme in complex orography. REF experiment produce convection almost correctly in the key areas (fig. 4.8 panel a)), but this convection, until 17:00 UTC, is shallow with hourly QPE not over 20 mm. The first and the second phase is represented with the correct timing and displaced only20-40 Km to the North. The last phase is represented to much west, even if, finally, the model QPE rise with quantitatives that reaches 45 mm with areal precipitation that finally rises as can be see in fig. 4.9 a) and in tab.4.2. Wind circulation is correctly represented for the direction, even if, winds are stronger than the real ones by more than 40 km/h, see Fig. 4.10 and CAPE has values around 2000-2500 J/kg, sensibly lower than the real ones.

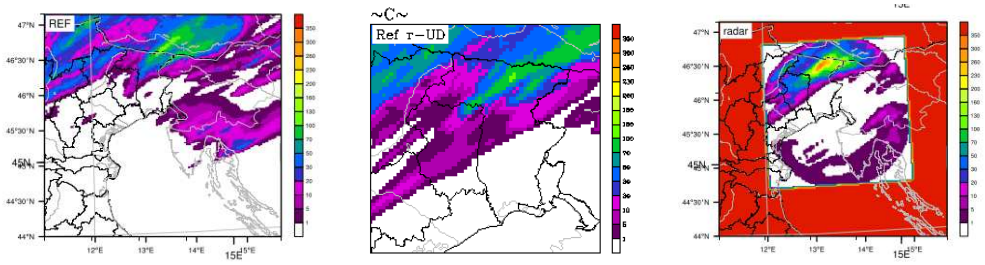

(a) REF (b) REF_R (c) RADAR

Figure 4.8: 24h accumulation of the Fella case for REF, REF_R experiments and RADAR.

Assimilation of radar measured precipitation bring to an increase of rain quantitatives, as can be seen in total values (Fig. 4.8 panel b)) and areal av-

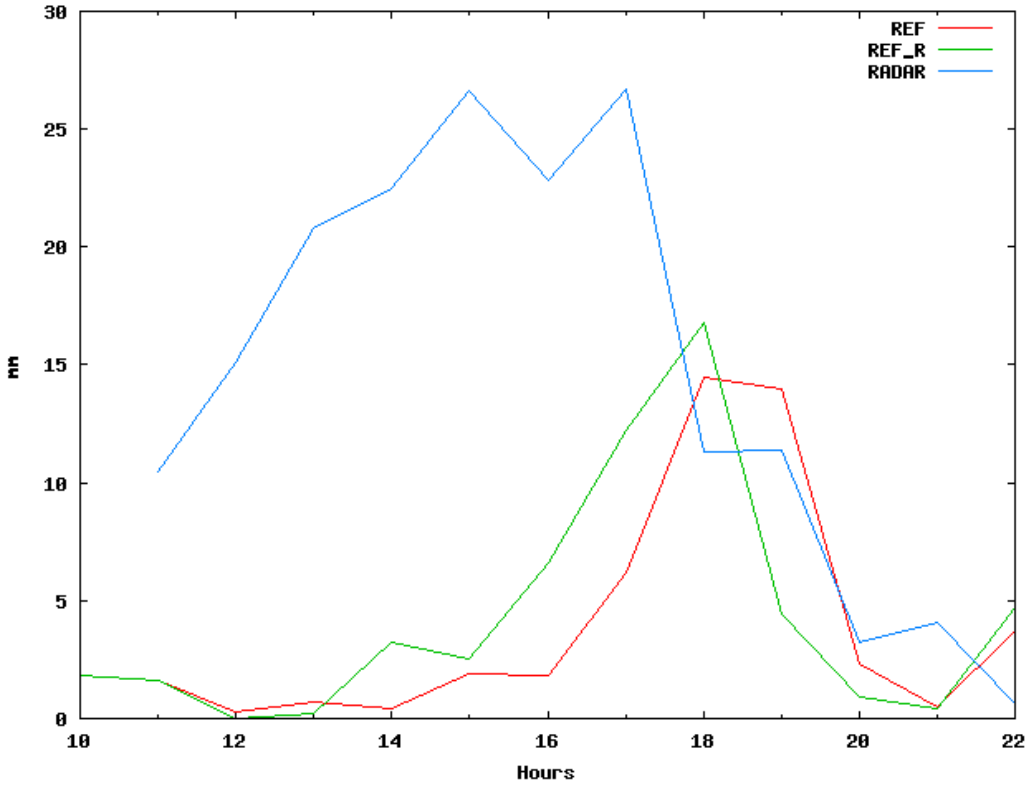

Figure 4.9: Time series of area-averaged hourly precipitation intensity (mm/h) derived from radar and simulations defined in Table 3 for the the Fella Basin .

Experiment	QP max(mm/h)	timing (UTC)	$\sum 24h(mm)$
RADAR	88.0	15:00 and 17:00	420.0
REF	45.0	18:00	112.0
REF_R	50.0	18:00	125.0
FC12	30	14:00	48
FC14	35	14:00	54
FC16	40	14:00	79
FC18	47	14:00	104

Table 4.3: Precipitation local peak accumulation for 23 August 2003: key figures of radar QPE, assimilation and forecast experiments in terms of hourly and 24-h accumulations and the corresponding timing.

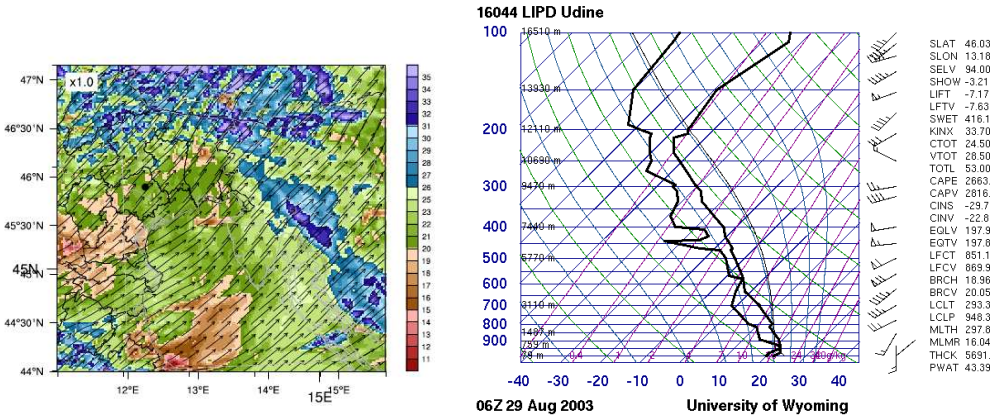

(a) (b)

Figure 4.10: Fella ref_r wind at 3000mt and 06:00UTC and Udine radiosounding

erages (Fig. 4.9). Some cells with precipitation higher than REF experiment are produced even before 17:00UTC, but quantitatives remained about 1/4 of the real ones. Timing and localization of the cell bands are ameliored with a correct positioning also of the third and last phases. Wind show some differences in the Fella area due to the presences of convective cells that brings to differences on circulation with mass moving due to updrafts.

Free forecast experiments show QPE maxima that varies from 30 to 47 mm/h increasing according with the number of hours of radar data assimilation, a similar behavior has the total event precipitation. Both the variables reaches with efforts and only with the longest radar data assimilation period the *REF* experiments values.

4.2.4 Statistical verification

Some statistical scores has been produced to comparate the performance of the model for both cases as can be seem in 4.11. POD (panel a)) show for the Mestre case values over the 80% of correctly "yes" events predicted with a rapid increase of the performance as the time flow and the rainfall is assimilated, this behaviour is present also on Fella case, even if with maximum values lower than for Mestre, but is clearly outkined the lack of the model to represent the first phases of the event. Panel b) show what fraction of the predicted "yes" events actually did not occur (i.e., were false alarms)

and is possible to see how the impact of LHN scheme is able to increase the performance of the model in the Mestre case, but seems to have lower inmpact on the second case. POFD, panel c), show, instedad, how the LHN forecast precipitation that is not really observed even if it not accounts for information on quantitatives that we no to be over 20 mm on 24 hours. Finally TS and ETS on panels d) and e)show higher values for Mestre case as was possible to expect. The TTS, panel f), that respond to the aswer "How well did the forecast separate the "yes" events from the "no" events?" show again a better behavior of the LHN on the first case, even if, after 16:00, it start to have good values also for Fella.

4.2.5 Summary and discussion

In summary, rainfall assimilation proves to be fast and efficient to reproduce the main features of the complex convective activity which occurred on 26 September 2007, as well as in suppressing unobserved convection present in the model simulation without rainfall assimilation. The rainfall assimilation was able to reproduce the area-averaged rainfall quite reasonably, but failed to simulate the locally observed rainfall peaks. The local peak rainfall maxima reached about 1/3 of the observed hourly and event accumulation close to 1/2 for the 24 hour accumulation. The forecast experiments for Mestre case are characterized by less intense convection and smaller rainfall accumulations over most of the north-eastern Italian domain. The realistically assimilated convective structures are not kept at the right intensity by the model. There is, however, a correct indication of how long these structures last. Probably forecasts FC_03 and FC_06, yielding some 70 and almost 140 mm in six and 24 hours, respectively, would have triggered an alert, or at least the forecaster's attention. It is noteworthy, that radar assimilation seems to feedback on the microscale structure of the atmospheric flow, where differences in details of the subsequent development of convection can be carried over into the free forecast for up to twelve hours and more.

The 23 August 2003 case has not been well represented by LHN scheme as the Mestre one, the rainfall assimilation bring ameliorment on timing and localization of precipitation, but lack on quantitatives. The local peak rainfall maxima reached about 1/4 of the observed accumulation. As for Mestre case, the forecast experiments show less intense convection and smaller rainfall accumulation, except FC_18 that has assimilated the most intese phase and is able to correctly predict the third one, probably no alert should be triggered by the various free forecasts.

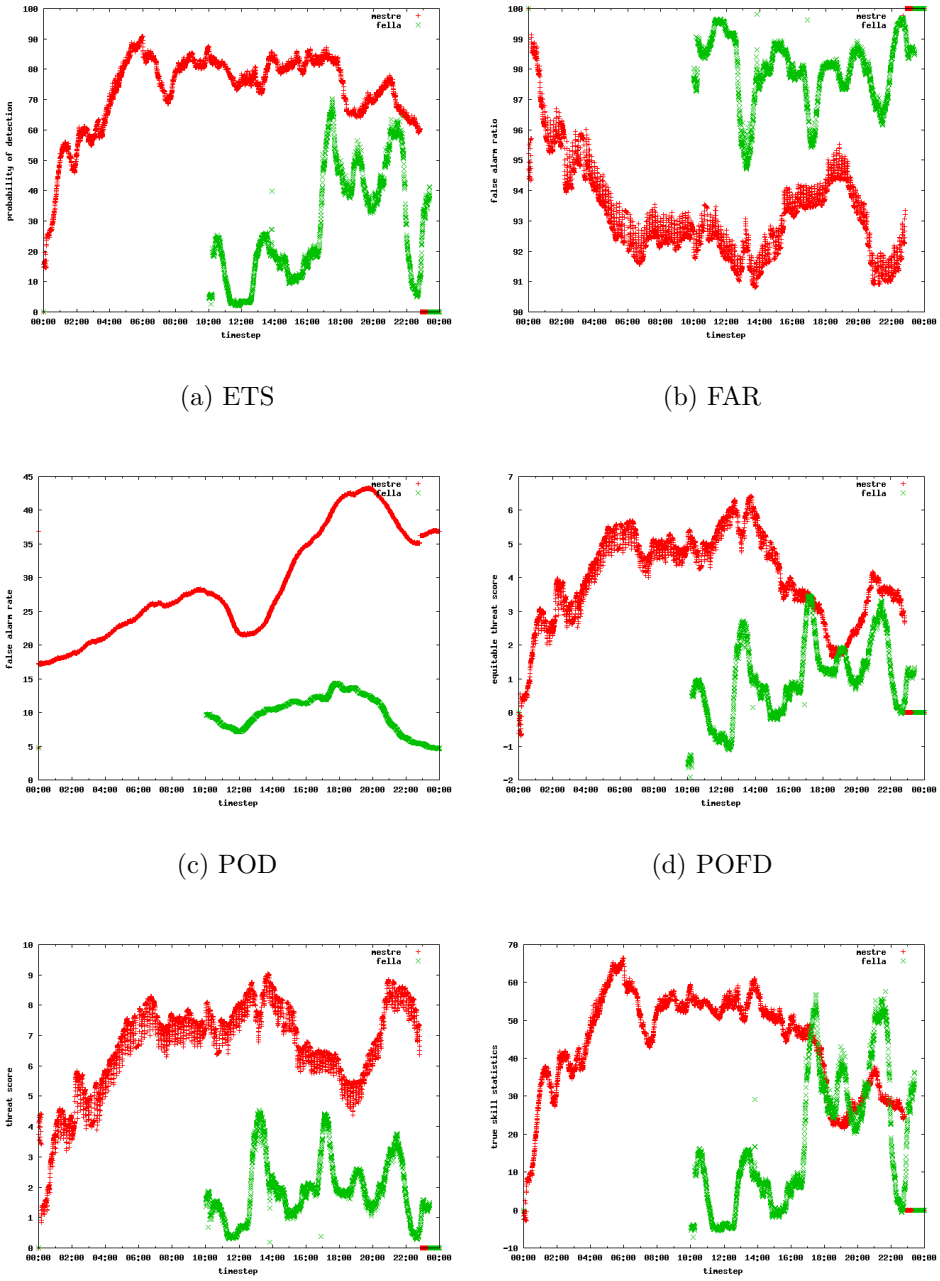

(a) ETS

(b) FAR

(c) POD

(d) POFD

(e) TS

(f) TSS

Figure 4.11: Statitistical scores for the REF_R experiments for Mestre and Fella cases.

Chapter 5

A new climatological profile for the COSMO-2 model

In this chapter the causes of loss of preformance of the LHN scheme for the Fella case are investigated and a new climatological profile is proposed.

5.1 Investigation on the LHN precesses for the Fella case

Latent heat nudge not optimal performance on the Fella flash flood representation has been investigated through comparison with Mestre case, an evaluation of the pre-convective enviromental conditions of the model and an accurate analysis of the LHN algorithm. The two cases had points of contact like:

- similar quantitative of precipitation produced (over than 400 mm).
- similar duration of the event, 24 hours with 6 of the more intense precipitation
- both the events were characterized by very deep and strong convection
- assimilation runs without LHN weren't able to correctly represent the events in timing and localization.

Differences can be resumed as:

- Fella basins was in complex orography
- Fella case had strong winds in altitude, Mestre showed a convergence on low levels.

- forcing due to rainfall measurements was continuos and localized always in the same places for Mestre case, Fella one was characterized by cells of the duration of 40-60 minutes that continuosly regenerates in the same areas

Prior to the development of convection, in the Fella area, the atmosphere was characterized by strong instability as evidenced by the very high CAPE value on the Udine radio sounding of 29 August 2003 at 0700 LST (about 4000 J/kg for the CAPE computed based on the most unstable parcel) associated with a low CIN. Precipitable water computed for this radio sounding amounts to 44 mm and shows that the humidity content of the atmosphere was already high. In the model representation the humidity content and the precipitable water were correctly computed but the cape not exceeded 2500 J/Kg with winds in altitude that reached 120 km/h (Fig. 4.6), 40 km per hours the real values.

Inspecting the LHN scheme is possible to note that for each grid point where the nudging is performed, if a compatible latent heat profile is not found (due to a too big difference between RR_{obs} and RR_{mod}), the scheme starts a 10 grid point (gp) radius search for profiles that corresponds to the correct characteristic. If this profile is found it also must soddisfy an height discriminance of $\Delta z = \pm 200$ that has bee chosen to avoid to assimilate profiles of places with great differences.

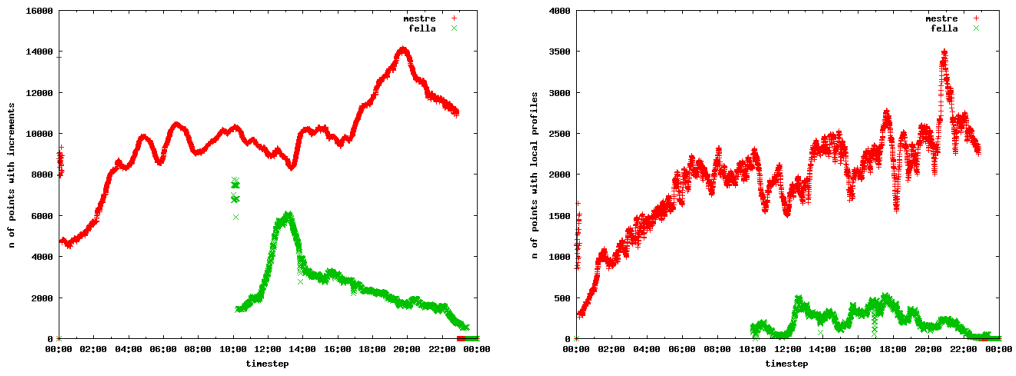

(a) (b)

Figure 5.1: a) :Number of grid points incremented.b) Number of local profile applied, red line is for Mestre case and Green one for Fella.

Fig. 5.1 panel a) shows the number of grid points that was subjected to a Laten Heat Nudging increments. These increments could be as positive

, related to the model precipitation forcing, as negatives, that are related to rain suppression. In Mestre case a large area of the domain is subjected to negative increments and this explain the higher number of grid points incremented, for Fella experiment is clearly visible how the radar assimilation try to force the model at the beginning of the rainfall. In panel b) is possible to note how for the Fella case the number of local profiles used is very low, the cause of this behaviour is to research in the too big difference between RR_{obs} and RR_{mod}, that is a discriminance for the choice of the local profile. At the end, if also this search bring any result, a climatological profile, that is hardcoded in the model, is applied.

In fig. 5.2 a) is clearly outlined that the Fella case has about 5 times of search failed than the Mestre case and these failed searches are expecially in the first and second phase of the event, in the third, that is represented in a better way by the model, has a number of fails reduced of the 60%. The most part of the failed search are due to the height dicriminance as can be easily seen on fig. 5.2 panel b) with values of about 70-90% of the total number, all of these GP are assimilated with the climatological profile.

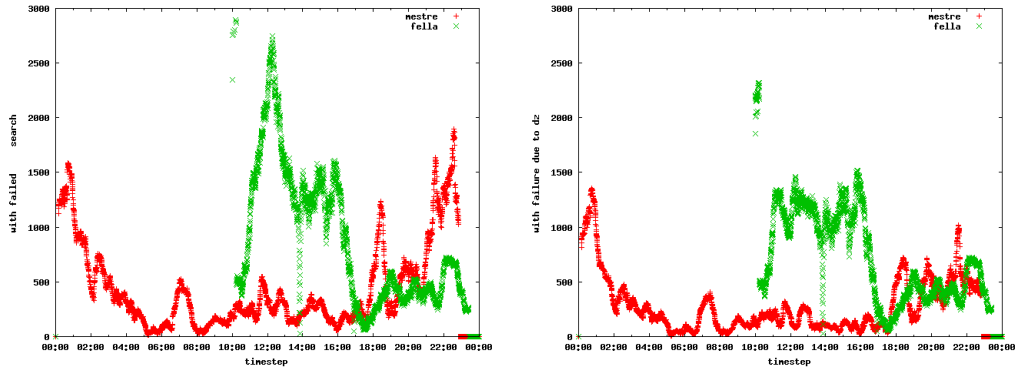

(a) (b)

Figure 5.2: Failed search of the LHN due to Δz and total for Mestre and Fella case, red line is for Mestre case and Green one for Fella.

5.2 A modified climatological profile

The COSMO-2 climatological profile (Fig. 5.3) seems to be slightly inadequate to force the model to start convection. As explained in capter 2, it

has been developed at DWD through several COSMO-2 runs (without LHN) that produced some statistics about latent heating profiles generated by the model and corresponding precipitation values, then it is applied without any evaluation of the interested area or of the season. So, this climatological profile is somewhat arbitrary and not based on a theory or similar.

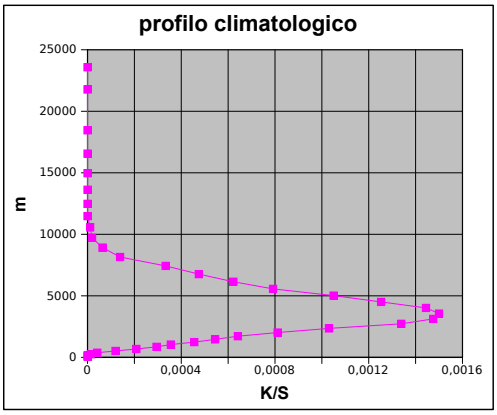

Figure 5.3: Cosmo-2 climatological profile of heating in K/s

It is easy to note from fig: 5.4 panel a) that the Italian Alpine and prealpine chains show values for the mean annual precipitation of more than 1500 mm, as can be seen for the Friuli Venezia Giulia (FVG) region on 5.4 panel b). This value is absolutely one of the highest for the COSMO-2 model domain (Fig. 5.4 panel a)) that in very large areas, with continental climate, has values less that 800-1000 mm for year. The shape, instead, is probably the best choice, due to its good similarity with real latent heating profiles (Tao et al. [2009]).

So, a statistic, "mean", climatological profile is probably not the best choice for Areas like the Fella Basin or the Alpine chains.

A climatological profile, modified in the intensity, but not in the shape has been tested for all the experiments in Tab. 4.2. The strength of the profile has been modified as in Tab.: 5.2. The choice to modify only the strength of the profile have been done after some preliminary studies that had shown a great instability of the model to other types of shapes.

5.3 Impact

An increase of the strenght of the COSMO-2 climatological profile in assimilation experiments brings to higher QPE starting from the REF_Rx1.001

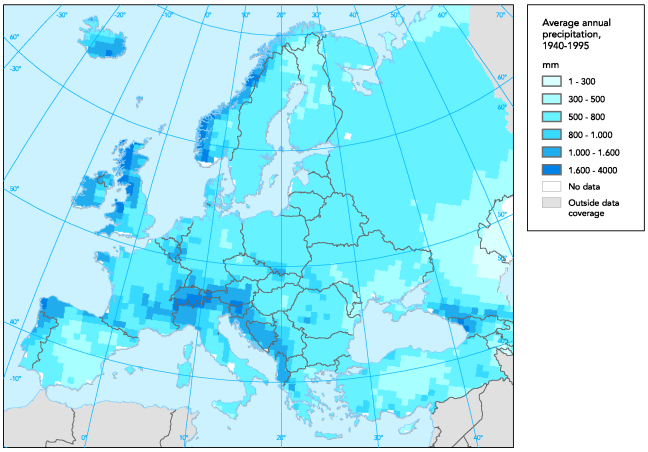

(a)

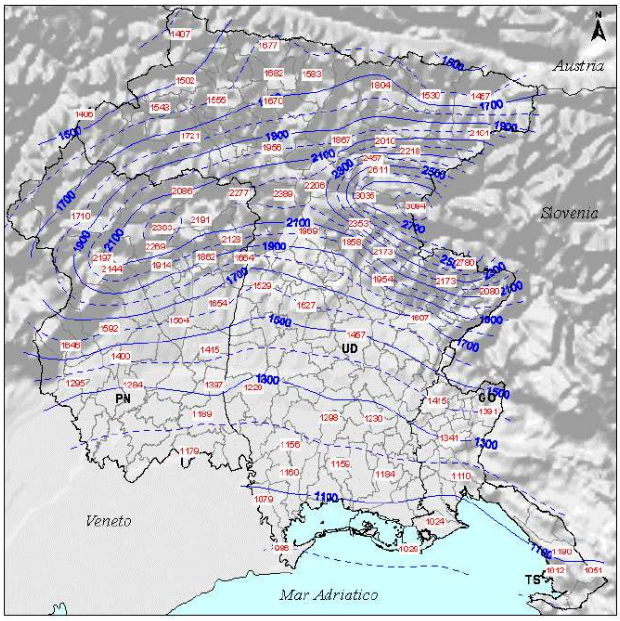

(b)

Figure 5.4: Mean annual precipitation for Europe and FVG

experiment(5.5), the values increase till REF_Rx1.05 then the growth became slower and total quantitatives don't change particularly. The total values of precipitation, as can be seen in 5.2, increase from 125 mm to 220-

Experiments	**description**
x0.8	Climatological profile reduced by 20%
x1.001	Climatological profile increased by 0.1%
x1,01	Climatological profile increased by 1%
x1.025	Climatological profile increased by 2.5%
x1.05	Climatological profile increased by 5%
x1.10	Climatological profile increased by 10%
x1.15	Climatological profile increased by 15%

Table 5.1: sensitivity experiments related wiith the LHN climatological profile

230 mm. The new climatological profile bring a better representation of the three phases of the storm, as can be seen with the localization of the maximum, even if it is placed some kilometers North-Eastern than in the real, and with the maximum that is set at 18:00. The other maximum at the Veneto region border is now present in the images, even if, as for the previous one, too north-eastern then the real one. During the first phases of the events, some cells are triggerend from the radar on the Adriatic sea with values that are higher than from the radar , 40 mm instead than 20 mm.

Experiment	QP max	timing (UTC)	$\sum 24h(mm)$
RADAR	88.0	15:00 and 17:00	420.0
REF_Rx1.0	50.0	18:00	125.0
REF_Rx1.001	53.0	18:00	150.0
REF_Rx1.01	58.0	14:00	183.0
REF_Rx1.05	68.0	14:00	222.0
REF_Rx1.10	70.0	14:00	230.0
REF_Rx1.15	73.0	14:00	239.0

Table 5.2: Precipitation local peak accumulation for 23 August 2003 for assimilation experiments with modified climatological profile: key figures of radar QPE, assimilation and forecast experiments in terms of hourly and 24-h accumulations and the corresponding timing.

Fig. 5.6 panel a) show results of area averaged precipitation that show how the modified profile bring a substantial increase on QPE, even if the total value is still the 50% of the radar quantitative. The temporal localization od the event is now much more realistic with an other peak at 14:00 UTC.

Statistical scores in figures 5.7 5.8 5.9 show the increasing of performance

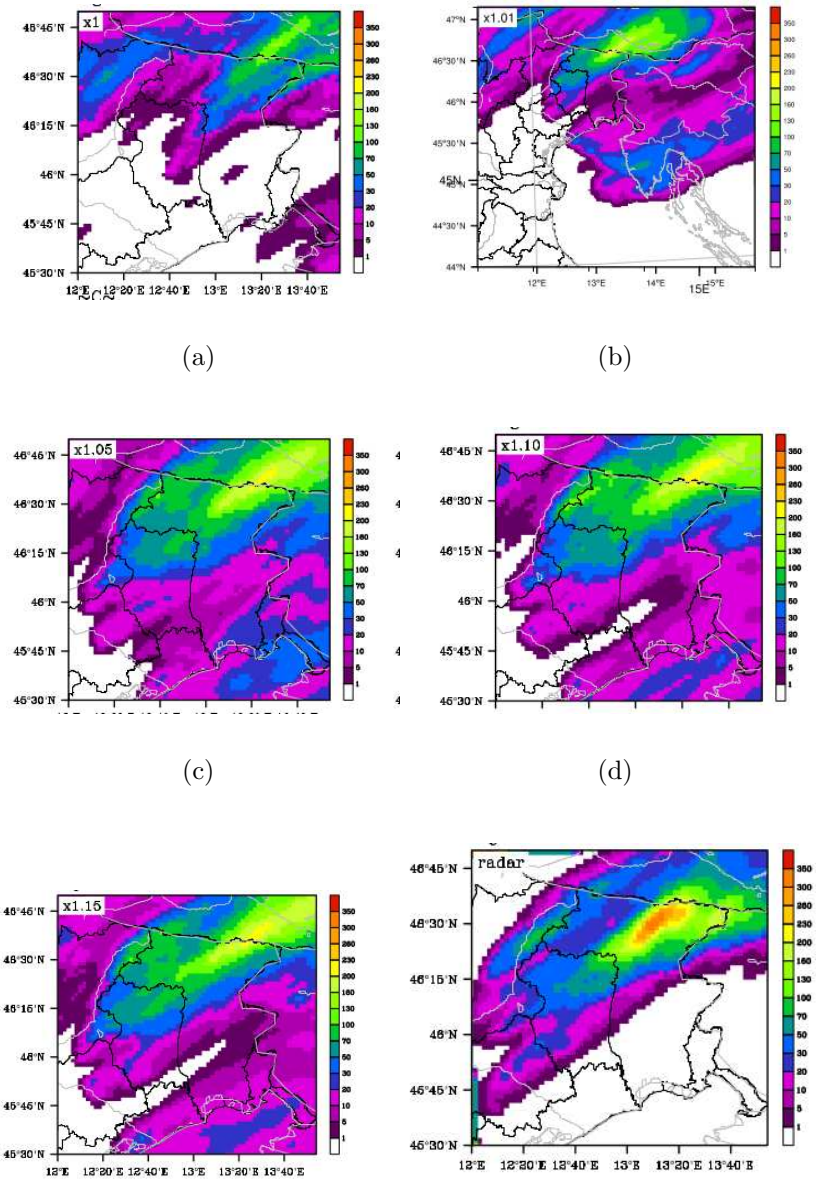

(a) (b) (c) (d) (e) (f)

Figure 5.5: 24-h precipitation for the various experiments

of the model on representing the event, expecially for the first phase. It is clearly outkined a step from REF_Rx1.01 experiment and a kind of convergence limit where REF_Rx1.05, REF_Rx1.10 and REF_Rx1.15 have similar

results. From about 18:00 performance became similar with all experiments

In particular POD and false alarm rate show how the modified profile is able to force the model rainfall with the correct spatial and temporal localization bringing to a performance ameliored of the 40%. Scores like HSS, TS and TSS show an increase of values 3-4 times all with the same behaviour and timing.

An inspection of the Latent Heat Nudging processes, Fig. 5.10, show that, till the 18:00 UTC, the number of failed search sensibly decrease, for values of 3000 to less tha 1000. Even the number of climatological profiles has the same behavior and similar values.

Other quantities as Wind, Humidity, Temperature are not generally modified by the new climatological profile (not shown).

For the free forecat experiments we will show only the x1.05 case because it is the value that has shown the better behaviour with an increase of performance and lower values of precipitation in the Adriatic region that x1.10 and 1.15.

Free Forecast experiments have shown(5.6 panel b)) a behaviour similar to the Mestre case with the skill to maintain convection for a period of 2-3 hours from the end of radar data assimilation as can be seen on areal averages and tab. 4.2. If the free forecast start in the middle of the second phase the model has performance similar to REF_R experiments with a little bit lower QPF, this can be related to the skill

5.4 Summary and discussion

In this section the Fella experiment not optimal behaviour has been investigated. In particular an accurate analysis of the LHN code has shown that the model isn't able to find an adequate Latent heat profile for a great number of grid point, expecially till in the first and second phase of the event. This is principally due to the complex orography of the area that force the model to choose the climatological profile a great number of times. This profile don't release in the atmosphere enough energy to trigger convection in the fundamental areas and so, results of the model are quite poor. A modified climatological profile has been tested, maintaining the similar shape but varing the strength of it.

An accurate valutation of the new profiles has brought to the choice of the one with a strength increase of the 5%, results has shown some beneficial impacts of it:

- QPE sensibly increased

- Areal averaged precipitation doubled respect the normal climatological profile
- Good temporal and spatial localization of the 3 phases of the storm
- QPF is increased, FC_16 show the skill to trigger convection for 4-5 hours after the end of assimilation, this can be related with a more realistic atmospheric representation by the model

The negative effects of the new profile can be categorized as follow:

- The model is more sensible to trigger convection and dealing with radar non-rain echoes can be problematic
- QPE and QPF are still quite smaller than from reality

In summary, this preliminary study show how much the climatological profile affects the results of the model, expecially in complex orography, and open the door to more accurate studies on this profile.

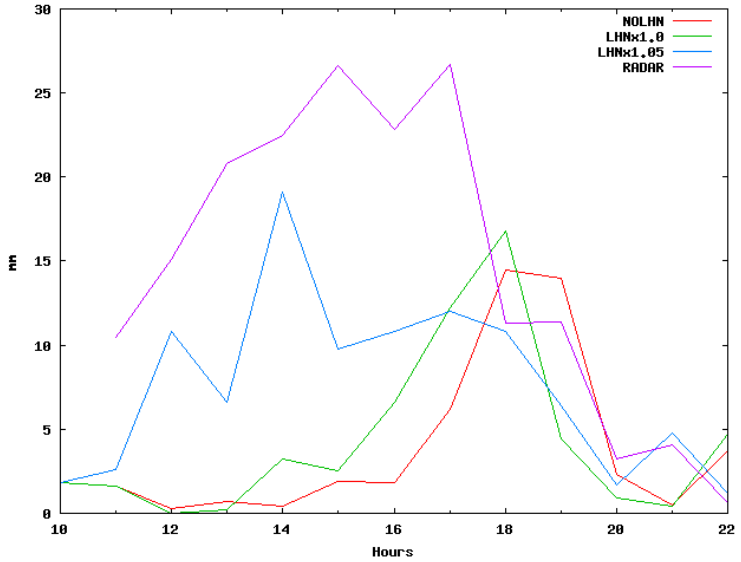

(a)

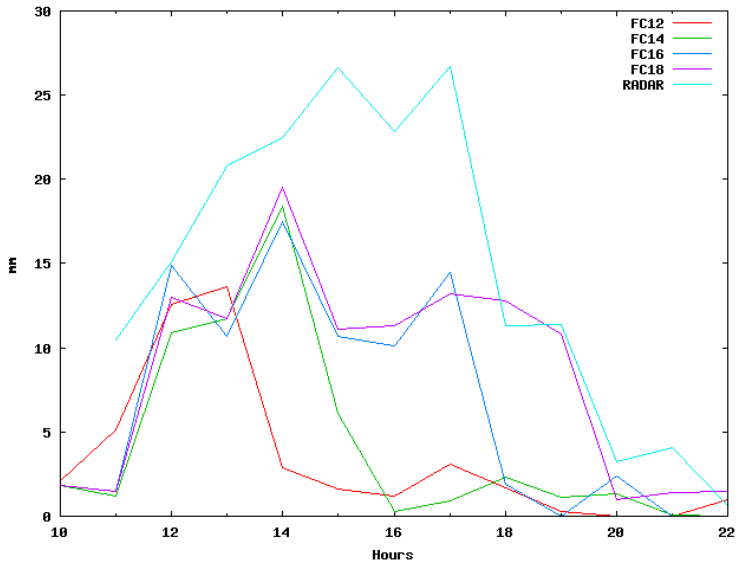

(b)

Figure 5.6: Time series of area-averaged hourly precipitation intensity (mm/h) derived from radar and simulations defined in Table 3 for the the Fella Basin.

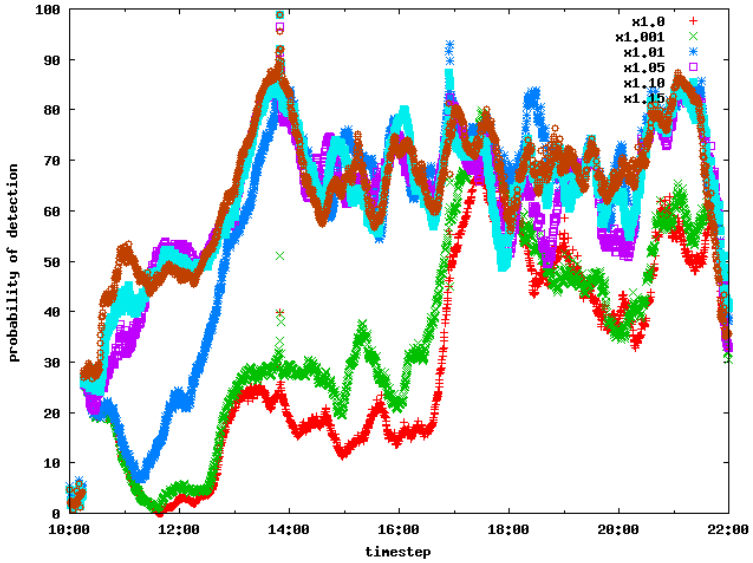

(a) POD

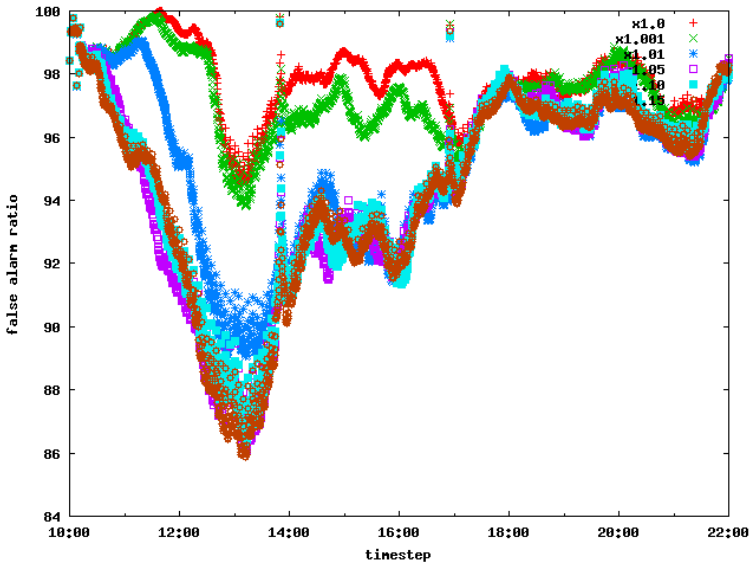

(b) FAR

Figure 5.7: Statitistical scores for the REF_R experiments with modified climatological profile for Fella case, red line is REF_Rx1, violet line is for REF_Rx1.05.

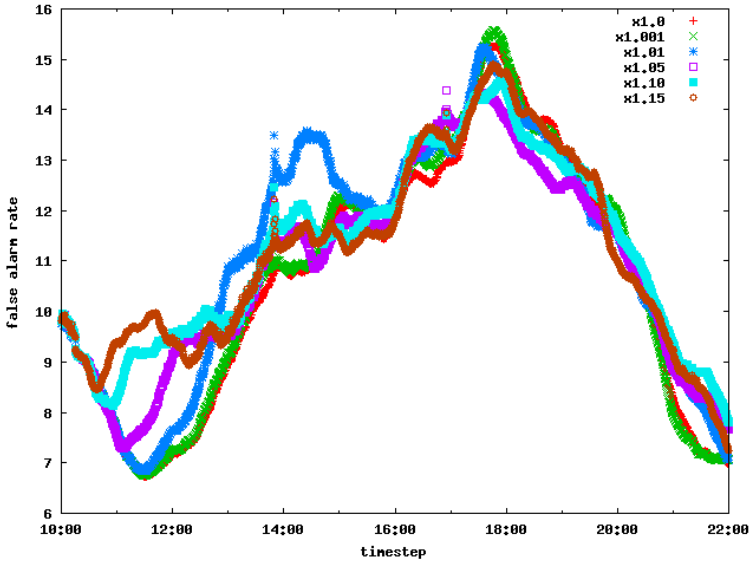

(a) POFD

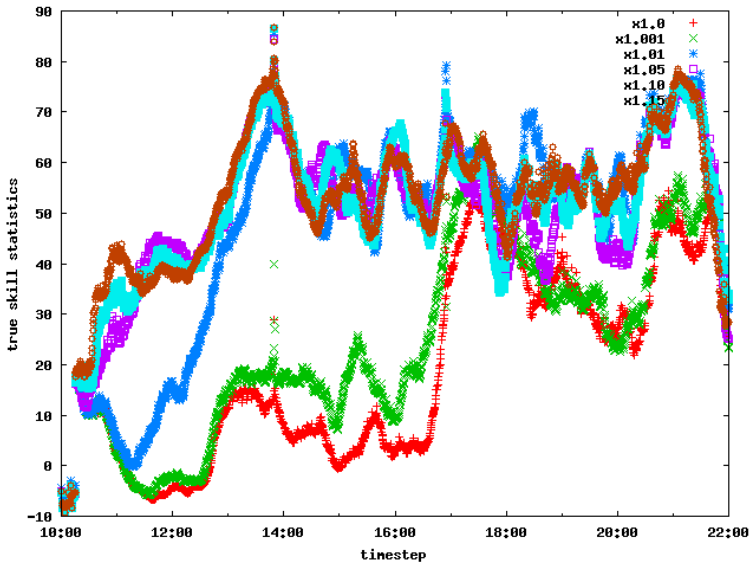

(b) TSS

Figure 5.8: Statitistical scores for the REF_R experiments with modified climatological profile for Fella case, red line is REF_Rx1, violet line is for REF_Rx1.05

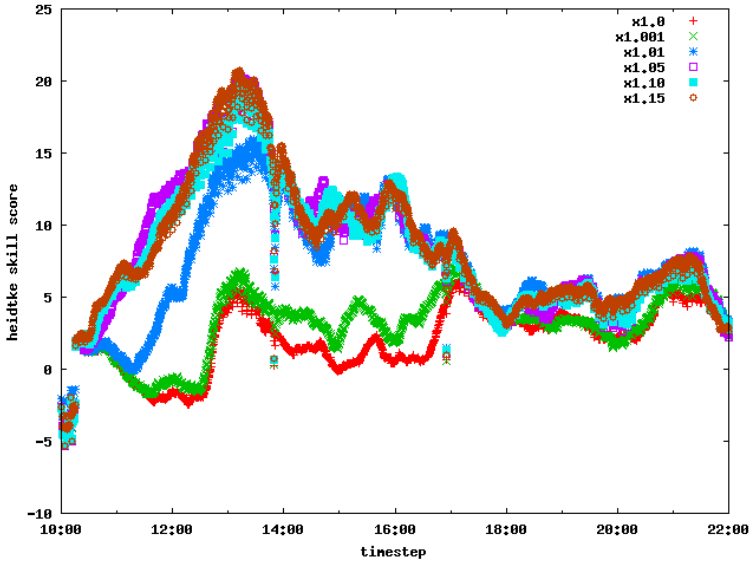

(a) HSS

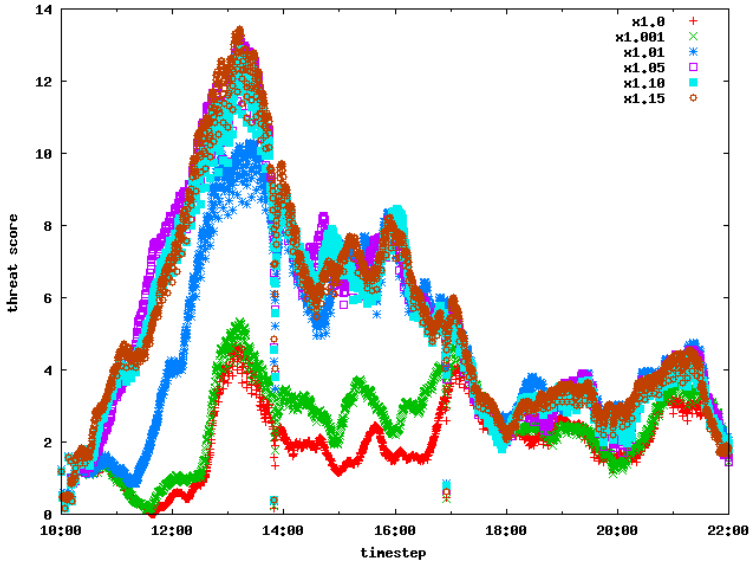

(b) TS

Figure 5.9: Statitistical scores for the REF_R experiments with modified climatological profile for Fella case,red line is REF_Rx1, violet line is for REF_Rx1.05

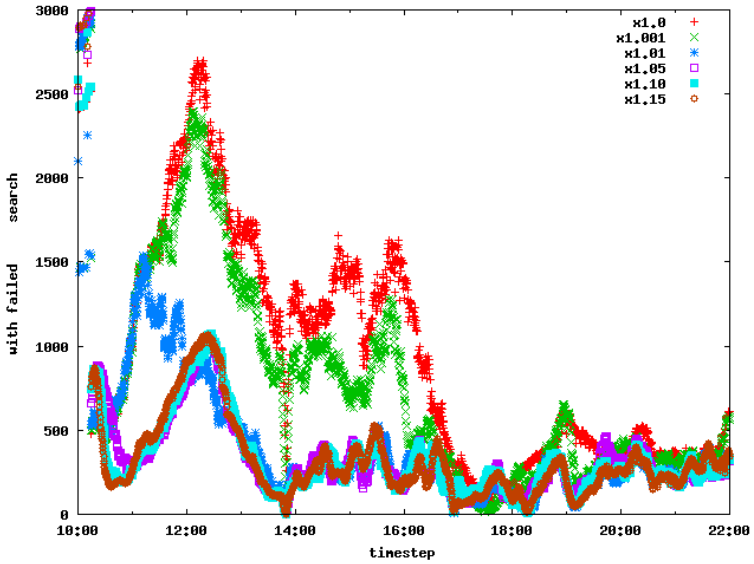

(a)

Figure 5.10: Failed search of the LHN algorithm (equivalent to the number of climatological profile used)

Chapter 6

An hydrologic application

In this chapter the 26 September 2007 Venice and the 23 August 2003 Fella flash floods are examined with a particular focus on radar data assimilation in order to evaluate whether extreme rainfall observations can be successfully inserted into the model's initial conditions and improve the ensuing forecasts.

6.1 The hydrologic and hydraulic models

The hydrological model used in this study is based on a semidistributed, continuous numerical scheme which couples the Green-Ampt approach for physically-based descriptions of both infiltration-excess and saturation-excess runoff generation processes and the Penman–Monteith model for the description of the evapo-transpiration fluxes. The mass balance equation is numerically solved at 1-h time step allowing a continuous update of soil moisture. Runoff propagation at the sub-catchment scale and over the river network is based on the geomorphologic transport approach (Rinaldo et al., 2006a,b; Botter et al., 2006; Settin et al., 2007). The basin is typically sub-divided into a suitable number of sub-catchments, characterized by uniform properties or parameters, including rainfall rate. The hydrological model is coupled with a one-dimensional hydrodynamic model. The coupling of the hydrological and hydraulic model is particularly relevant for the study area, where a significant portion of the channel network (including the location of the streamgauges) is affected by the tidal influence.

6.2 Hydrological simulations

In this section, the hydrological simulations obtained by using the rainfall input from the radar QPE, as well as the NWP QPF are presented and

Figure 6.1: Domain of the semi-distributed geomorphological hydrological model for the river Dese catchment. The main river network and the partitioning into small sub-catchments is shown; the streamgauge station is located near the town of Dese.

discussed

6.2.1 Mestre case

The hydrological-hydraulic model is used for the simulation of the Dese (Fig. 6.1) river catchment, a 90 km^2 basin discharging into the Venice lagoon, that was the basins were the MCS insisted.

Fig. 6.2 shows the hydrographs for the rainfall experiments reported in Tab. 4.2 while fig:6.3 shows the Dese catchment-averaged rainfall intensity (mm/h). Table 6.1 reports key quantities concerning rainfall from the various simulation experiments and the corresponding runoff simulations for the Dese basin. The variables reported in Table 6.1 are: areal cumulated precipitation (mm), hourly areal maximum precipitation (mm) and corresponding timing (hour of the day), as well as peak flow ($\frac{m^3}{s}$) and corresponding timing.

Fig. 6.6 shows that the runoff simulation obtained from the radar rainfall is reasonably good, in that it reproduces correctly the essential features of the measured hydrograph. The peak flow value is predicted very well, with a 2% error with respect to the observed value. There is however an overall 1 h and half anticipation of the simulated hydrograph with respect to the observed

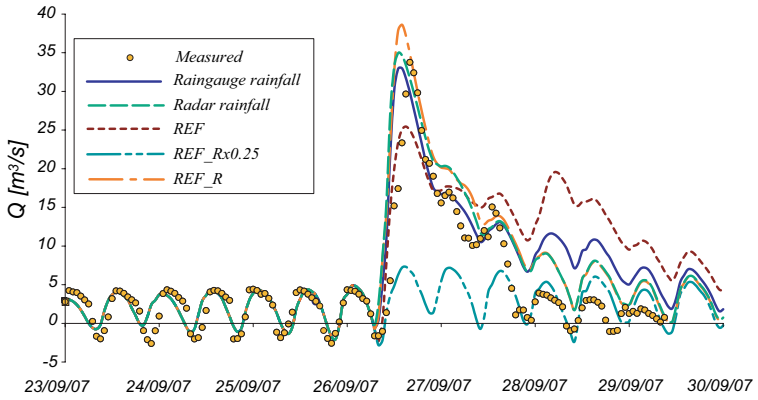

(a)

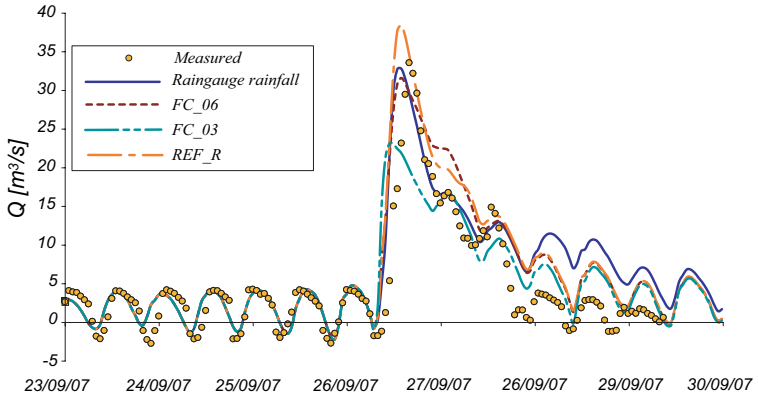

(b)

Figure 6.2: Observed and simulated discharge time series for the Dese catchment at Dese for different precipitation input: (a) observed and simulated discharges obtained from radar and assimilation experiments; (b) as in (a) but precipitation input from forecast experiments as defined in Table 4.2.

one. Note also the strong influence of tidal fluctuations,which is evident especially during dry periods. The reference simulation (REF), consistent with the NWP QPF, confirms the strong underestimation of rainfall volumes during the MCS phase of event, as well as the incorrect overestimation of the rainfall during the afternoon and the evening. These discrepancies combine to underestimate the peak discharge of the 26 September and to generate a persistent moderate discharge during the subsequent days.

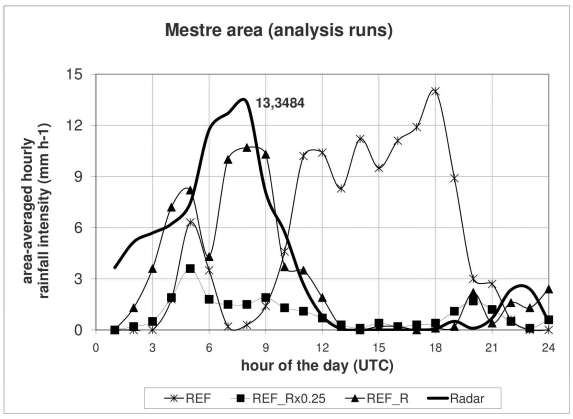

(a)

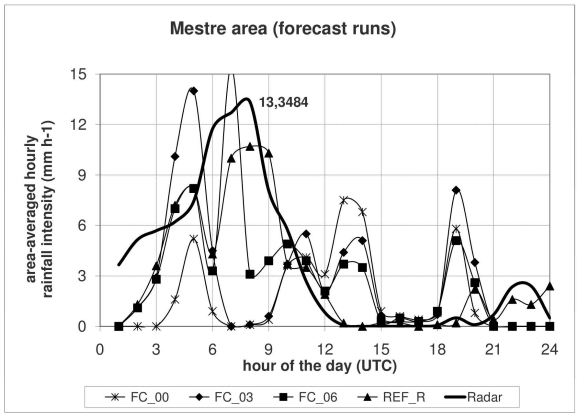

(b)

Figure 6.3: Dese catchment-averaged rainfall intensity (mm/h) corresponding to the performed experiments as defined in Table 4.2.

Assimilation of the radar QPE in the REF_R experiment dramatically

Experiment	QP max (mm)	timing (UTC)	$\sum 6h(mm)$	$\sum 24h(mm)$	Peak flow
Observed peak flow	125.0	07:00	290.0	324	32.99
RADAR	159.0	07:00	328.0	410.0	35.5
REF	28.0(65.0)	05:00 (15:00)	32.0	140.0	25.4
REF_R	41.0	06:00	108.0	265.0	38.6
FC00	19.0(36.0)	05:00 (20:00)	19.0	90.0	11.7
FC03	43.0(37.0)	05:00 (20:00)	65.0	101.0	23.3
FC06	32.0 (25.0)	04:00 (19:00)	72.0	137.0	31.3

Table 6.1: Cumulated areal quantitative precipitation (QP), hourly areal maximum precipitation and timing, as well as peak flow and timing. Values in brackets for the areal QPmax and its timing indicate the evening peak in the simulations which was not actually observed.

improves the quality of the modeled hydrograph which is inreasonable agreement with the observed discharge. The simulated peak discharge is overestimated by 14% and anticipated by 2 h. Note that the inability of REF_R to reproduce the local rainfall peak proved immaterial to the correct simulation of the hydraulic response in this complex watershed. Provided that the typical size of sub-basin is smaller than the characteristic size of rainfall patterns, the rainfall spatial structure effectively samples all possible residence times and basin's heterogeneity and the response of the catchment does not depend on the specific rainfall pattern (Nicotina et al., 2008; Zoccatelli et al.,2010). Fig. 6.4 shows that the sensitivity experiments performed by scaling the radar rainfall amplitude propagate quite linearly through the hydrological simulations, except for the two lowest radar QPE scaling factors, for which the rainfall over the Dese catchment probably are insufficient to generate significant runoff(e.g. REF Rx0.25 in Fig.6.4). Also, a slightly non-linear response of the basin is apparent for the highest rainfall.

Fig. 6.6 b) shows the hydrographs simulated with the COSMO-2 forecast experiments together with the observed hydrograph. For the sake of comparison the hydrographs simulated with the radar QPE and the REF_R QPF are also included in the figure. It is encouraging to observe that there is substantial improvement in the flood prediction from experiment FC_00 to FC_03 and then to FC_06 with a peak flow increasing from 11.7 to 21.3 and then to 31.7 m3 sÀ1, which have to be compared with an observed value of 33.8 m3 sÀ1. A similar trend may be observed for the forecast of the peak discharge timing. Both these observations show that the location information provided by assimilating the radar rainfall observations contribute to improving significantly the river flow forecasts.

In the perspective of a rapid update cycle, in which the NWP QPF is up-

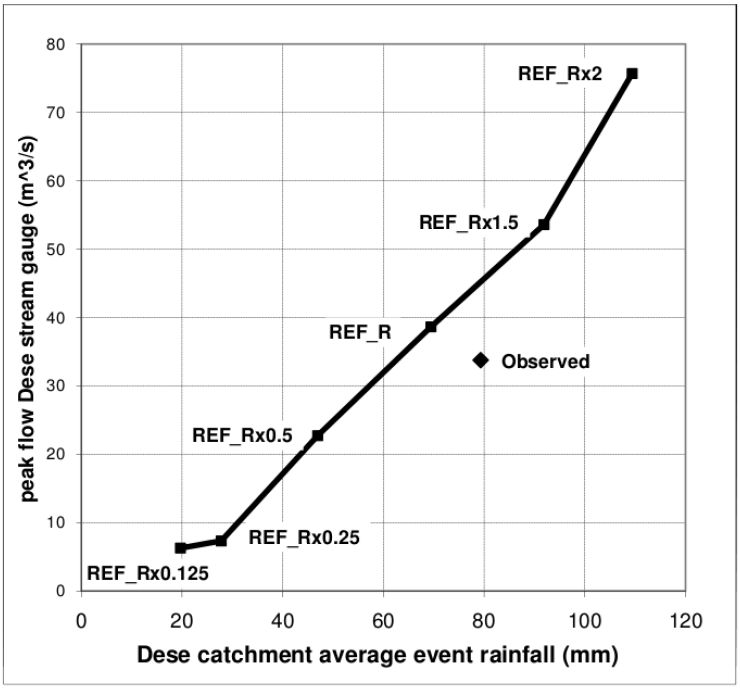

Figure 6.4: Relationship between the catchment event rainfall produced by the NWP assimilation sensitivity experiments as defined in Table 3 and the corresponding simulate peak discharge at the Dese streamgauge station. The observed peak discharge is also reported.

dated more frequently than what is traditionally done, such an improvement becomes extremely valuable. When considering the free forecast FC_06, the warning lead time, computed as the distance in time between the forecast issue time and the observed peak discharge, is around 10 h. The corresponding lead time available when using only the real-time observed rainfall (i.e., without any input from NWP models) is 7 h (details of the computation not reported here). Therefore, assimilating radar rainfall into the NWP model affords an extension of lead time by 3 h for this case study. This extension may represent extremely valuable information for a more effective response to the event and to minimize the effects of the ensuing flash flood, taking into ac- count that it takes considerable time to disseminate the warnings to the users. Clearly, this coupling of prediction models extends the lead time for users but also further increases the uncertainty in the forecasts (Siccardi et al., 2005) and further efforts are required to quantify the uncertainty and optimize decisions (Martina et al., 2006).

6.2.2 Fella case

The 29 August 2003 storm on the upper Tagliamento River basin (Fig 6.5) is examined here as a prototype for organized convective systems that are likely responsible for the majority of flash flood peaks in this area of the eastern Italian Alps.

During the August 2003 flood, exceptional rainfall rates and accumulations were observed on the right hand tributaries of the Fella, whereas the left-hand tributaries received much less rainfall, imposing a contrasting flood response to the different elements of the river system. On 28 August 2003, the day before the flood, a localized convective storm generated almost 100 mm of precipitation on areas of the left-hand tributaries of the Fella River system. This added to the various nonlinearities sources in the hydrologic response, introducing elements of spatial variability in the pattern of antecedent soil moisture conditions.

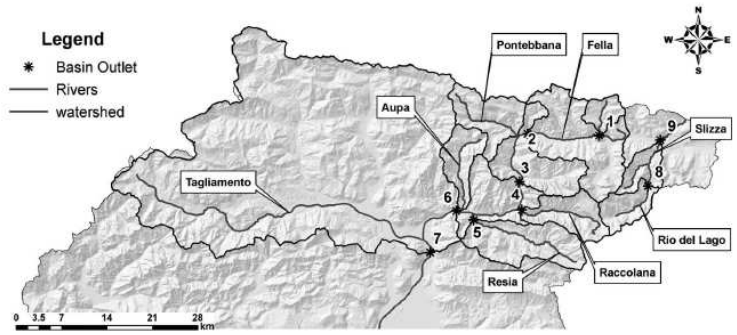

Figure 6.5: Catchment map of the upper Tagliamento River basin, with subcatchments of the Fella River basin: 1) Uqua at Ugovizza; 2) Fella at Pontebba; 3) Fella at Dogna; 4) Raccolana at Raccolana; 5) Resia at Borgo Povici; 6) Fella at Moggio Udinese; 7) Tagliamento at Venzone; 8) Rio del Lago at Cave del Predil; 9) Slizza at Tarvisio.

Assimilation of of rainfall QPE of the REF experiments show very low values, with a peak of $90 m^3 s^{-1}$, for the simulated hydrograph with a simulated discharge peak that is 1/10 of the real value, Latent Heat Nudging don't improve very much the performance of the model with the value of the peak that increase only a little respect to the REF experiment (Fig 6.6 a), b)). This behaviour is coherent with the large underestimation and the not perfect localization of the event with the peak placed 20-30 Km north-eastern, in a different basin.

Experiment with the modified climatological profile, in spite of the more than doubled areal-average precipitation, show (Fig. 6.6 c)) a simulated

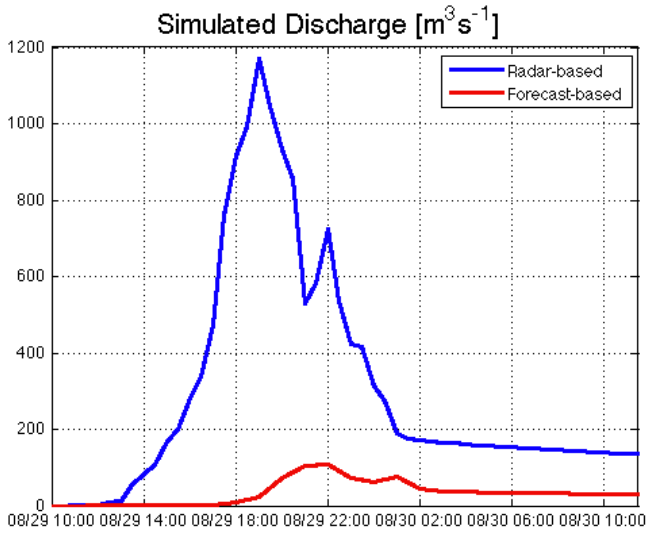

(a)

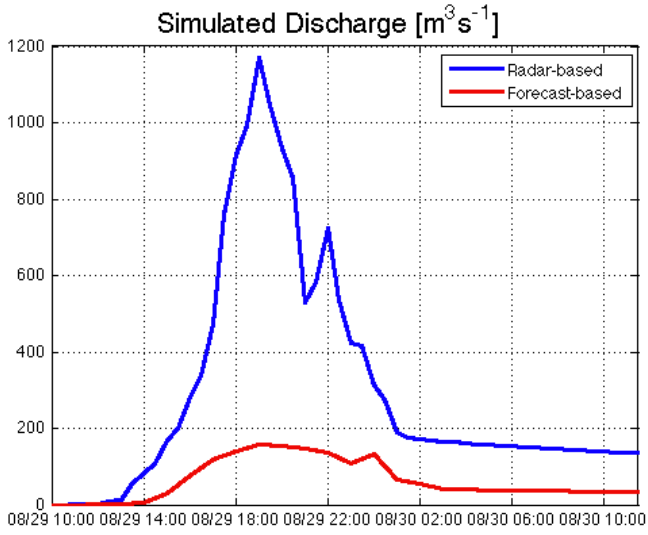

(b)

Figure 6.6: Observed and simulated discharge time series for the Fella basin for different precipitation fro REF_R and REF_Rx1.05 experiments.

discharge rate that rise not linearly, remaining under $200 m^3 s^{-1}$ for the maximum peak value.

This non-linear response of the model can be related principally with the extremely warm and dry period before the event that brought to a very dry soil condition that the model hasn't been able to correctly represent.

Due to this not optimal response of the hydrological model to the COSMO-2 precipitation quantitatives, that shouldn't bring to any Hydrologic warning (even if a Meteorological warnig should be emitted due to the rain amounts) has been reputated not necessary to run free forecast experiment.

6.3 Summary and discussion

In this chapter an application of the radar rainfall assimilation into an high resolution atmospheric model is shown for 2 flash flood cases that wasn't well represented by the model.

For the Mestre case the hydrologic validation confirms the benefit of assimilating the radar information in the NWP analyses and forecasts. The simulated peak flow obtained by using rainfall resulting from the assimilation experiments matches well the observed data both in value and in its timing. The best hydrological forecast is obtained by using assimilation which includes the main MCS in an already developed stage. In this case, assimilating radar rainfall into the NWP model affords an extension of lead time by 3 h.

Impact of the radar data assimilation for the Fella case is not so beneficial, even with the modified climatological profile. The simulated peak flow matches well in timing with observed data, but values are considerably lower than from measures with a non linear behaviour. In this case, assimilationg radar data not bring to any Hydrologic warnig of the model

Chapter 7

Further remarks

7.1 Synthesis of the results

In this study, the convective capabilities of the Latent Heat Nudging scheme have been evaluated and improved. In particular, an empirical quality description of radar derived QPE has been extensive evaluated in Chapter 2, and Chapter 3 is dedicated to the evaluation of the convective capabilities of the LHN scheme for 2 case studies, characterized by very intense precipitations. A modified climatological profile is proposed and evaluated in Chapter 5 and, finally, an hydrological application of the QPE and QPF of the COSMO-2 model is presented in Chapter 6.

The variety of findings are summarised and discussed at the end of the corresponding chapter. Here, the main results are assembled and future perspectives are outlined.

- the radar data quality function has shown small but consistent improvement of COSMO-2 precipitation analysis with beneficial impacts on reduction of artifacts and rest clutter identification. It is easy to construct and simple to use, but it reproduces the main error structures and is, therefore, a plausible way to account for problems normally found in radar QPE. At the end it can 'easily' be evaluated for different radar networks and, potentially, also for heterogeneous networks.

- the LHN assimilation scheme proves to be very efficient in reproducing the main features of the complex convective activity in simple orography, suppressing unobserved convection present in the model simulation without rainfall assimilation, and reproducing the area-averaged rainfall quite reasonably. For the case in complex orography and short-time forcing, LHN has shown quite good spatial and temporal agree-

ment with observation, but the precipitation quantitative are 1/4 of the observed.

- the lack of LHN peformance for the complex orography case can be related with the massive use of the climatological profile of the scheme, due to the height discriminance. The modified climatological profile has shown some improvement in representing the event, with a sensible increase of the precipitation quantitatives, but the area-averaged values are still 1/2 of observed.

- Sensitivity to the amplitude of the assimilated rainfall shows that the NWP response is generally quite linear to the forcing, but not capable of reaching the observed intensities for the main MCS. During and after the most intense phase of the convective activity, non-linear effects induce differences in the details of the convective structure among the various experiments.

- The positive impact of the rainfall assimilation in analysis mode is carried over into the free forecast mode for about 2–5 h, depending on when the forecast is started. After this time the upper-level dynamics, largely unaffected by the rainfall assimilation, re-introduces the incorrect precipitation systems present in the reference simulation, thus pinpointing the limitation of the LHN in modifying the mesoscale dynamics, especially at upper levels. Some benefits, especially in terms of reduced incorrect precipitation, are observed up to some 10 h into the free forecast.

- The hydrologic validation confirms the benefit of assimilating the radar information in the NWP analyses and forecasts, even if a lot of work needs to be done. The simulated peak flow obtained from the assimilation experiments matches well the observed data both in value and in its timing. The best hydrological forecast is obtained by using assimilation which includes the main MCS in an already developed stage. In this case, assimilating radar rainfall into the NWP model extends lead time by 3 h.

Bibliography

Kouwen N. Yu W. Benoit, R., S. Chamberland, and P. Pellerin. Hydrometeorological aspects of the real-time ultrafinescale forecast support during the special observing period of the map. *Hydrol. Earth Syst. Sci.*, 3, 2003.

M. Berenguer and I. Zawadzki. A study of the error covariance matrix of radar rainfall estimates in stratiform rain. *Weather and forecasting*, 2008.

M. Berenguer, C. Corral, R. Sanchez-Diezma, and D. Sempere-Torres. Hydrological validation of a radar-based nowcasting technique. *J. Hydrometeorol*, 2005.

Binder P. Buzzi A. Dirks R. Houze R. Kuettner J. Smith R.B. Bougeault, P., R. Steinacker, and H. Volkert. The map special observing period. *Bull. Am. Meteorol. Soc.*, 82, 2001.

K. Chancibault, Ducrocq V. Anquetin, S., and G.-M. Saulnier. Hydrological evaluation of high-resolution precipitation forecasts of the gard flash-flood event (8 and 9 september 2002). *Quarterly Journal of the Royal Meteorological Society*, 132, 2006.

C.G. Collier. Flash flood forecasting: what are the limits of predictability? *Quarterly Journal of the Royal Meteorological Society*, 2007.

J. William Conway, Chip Barerre, Gabriele Formentini, Luciano Lago, Andrea Rossa, and Michela Calza. Flash flood prediction in italy: Development and testing of a new capability. In *Proceedings of 21st Conference on Hydrology*. AMS Annual, AMS, January 2007. URL `http://ams.confex.com/ams/pdfpapers/121128.pdf`.

S. Davolio, D. Mastrangelo, M. M. Miglietta, O. Drofa, A. Buzzi, and P. Malguzzi. High resolution simulations of a flash flood near venice. *Nat. Hazards Earth Syst. Sci.*, 9(5):1671–1678, October 2009. ISSN 1561-8633.

G. Doms and U. Schättler. A description of the nonhydrostatic regional model LM: Part I: Dynamics and numerics. available from http://cosmo-model.org, 2002.

K.K. Droegemeier. The numerical prediction of thunderstorms: challenges, potential benefits and results from real-time operational tests. *WMO Bull*, 46, 1997.

E.E. Eberth. Fuzzy verification of high-resolution gridded forecasts:a review and proposed framework. *Meteorol. Appl.*, 15:51–64, 2008.

A. Fornasiero, P. P. Alberoni, R. Amorati, and C. Marsigli. Improving the radar data mosaicking procedure by means of a quality descriptor. In *ERAD Publication Series*, volume 3, pages 378–341, 2006.

K. Friedrich and M. Hagen. Wind Synthesis and Quality Control of Multiple-Doppler-Derived Horizontal Wind Fields. *Journal of Applied Meteorology*, 43:38–57, 2004. URL .

G. A. Gal-Ghen and C. J. Sommerville. On the use of a coordinate transform for the solution of the navier-stokes equations. *J. Comput. Phys..*, 1975.

Germann and Joss. Operational measurement of precipitation in mounatinous terrain. *In Weather Radar: Principles and advanced applications, P. Meischner*, Springer Series, Physics of Earth and Space Environments: 52–75, 2004a.

G. Galli M. Boscacci M. Bolliger Germann, U. and M. Gabella. Quantitative precipitation estimation in the alps: where do we stand? *ERAD Pubblication Series*, 2:2–6, 2004.

U. Germann and J. Joss. *Weather Radar: Principles and Advanced Applications', edited by P. Meischner in Springer monograph series 'Physics of Earth and Space Environment'*, hardcover Operational measurement of precipitation in mountainous terrain, page 337pp. Physics of Earth and Space Environment. Springer, 2004b.

U. Germann, G. Galli, M. Boscacci, and M. Bolliger. Radar precipitation measurement in a mountainous region. *Quarterly Journal of the Royal Meteorological Society*, 132:1669–1692, 2006.

J.J. Gourley, J. Zhang, R. A. Maddox, C. M. Calvert, and K. Howard. A real-time precipitation monitoring algorithm - quantitative precipitation estimation and segregation using multiple sensors (qpe-sums). In *Preprints,*

Symp. On Precipitation Extremes: Predictions, Impacts, and Responses., pages 57–60. AMS, AMS, 2001. Albuquerque, NM.

I. Holleman, D. Michelson, G. Galli, U. Germann, and M. Peura. Quality information for radars and radar data (opera document available at http://www.knmi.nl/opera). EUMETNET OPERA document, 2006. URL `www.opera.nl`.

C. D. Jones and B. Macpherson. A latent heat nudging scheme for the assimilation of precipitation data into an operational mesoscale model. *Meteorol. Appl.*, 4:269–277, 1997. URL .

J. et al. Joss. Operational use of radar for precipitation measurements in switzerland. Technical report, NRP 31, vdf Hochschulverlag an der ETH Zuerich, 108 pp., ISBN 3 7281 2501 6, 1998.

E. Kalnay. Atmosphere modelling, data assimilation and predictability. *Cambridge university press*, 2003.

R. J. Keeler and S. M. Ellis. Observational error covariance matrices for radar data assimilation. *Physics and Chemistry of the Earth, Part B: Hydrology, Oceans and Atmosphere*, 25(10-12):1277 – 1280, 2000. URL `http://www.sciencedirect.com/science/article/B6VPV-41F63DT-35/2/3f139a35a6ac58`

F. Laudanna Del Guerra. Construction of an empirical radar data quality function and analysis of its impact on radar data assimilation. Master's thesis, University of Bologna, 2010.

D. Leuenberger and A. Rossa. Revisiting the latent heat nudging scheme for rainfall assimilation of a simulated convective storm. *Meteorology and Atmospheric Physics*, available online:25pp, 2007.

P.W. Li and E.S.T. Lai. Short-range quantitative precipitation forecasting in hong kong. *J. Hydrol*, 2004.

D.K. Lilly. Numerical prediction of thunderstorms-has its time come? *Quart. J. Roy. Meteorol. Soc.*, 116, 1990.

B. Macpherson, M. Lindskog, V. Ducrocq, M. Nuret, G. Gregoric, A. M. Rossa, G. Haase, I. Holleman, and P. P. Alberoni. Quality and assimilation of radar data for nwp. *In Weather Radar: Principles and advanced applications, P. Meischner*, Springer Series, Physics of Earth and Space Environments:255–279, 2004.

D. Michelson, T. Einfalt, I. Holleman, U. Gjertsen, K. Friedrich, G. Haase, M. Lindskog, and J. Szturc. Weather Radar Data Quality in Europe: Quality Control and Characterization. *ERAD-3, Visby, Sweden, 6-10 September 2004*, 2004. URL .

M. Monai, A. M. Rossa, and A. Bonan. Detailed study of a north Adriatic frontal passage and related partitioning of snowy and rainy precipitation. *Advances in Geoscience*, 7:279–284, 2006.

Jones D.A. Moore, R.J., D.R. Cox, and V.S. Isham. Design of the hyrex raingauge network. *Hydrol. Earth Syst. Sci.*, 4, 2000.

Borga M. Esposti S.D. Gaume E. Anquetin S. Norbiato, D. Flash flood warning based on rainfall thresholds and soil moisture conditions: an assessment for gauged and ungauged basins. *Journal of Hydrology*, 2008.

Daniele Norbiato, Marco Borga, Marco Sangati, and Francesco Zanon. Regional frequency analysis of extreme precipitation in the eastern Italian Alps and the August 29, 2003 flash flood. *Journal of Hydrology*, 345:149 – 166, 2007.

A.. Rossa and D. Leuenbeger. Sensitivity of the lhn scheme to non-rain echoes. *Meteorological Applications*, 15:503–511, 2008.

A. Rossa, K. Liechti, M. Zappa, M. Bruen, U. Germann, G. Haase, C. Keil, and P. Krahe. Uncertainty propagation in advanced hydro-meteorological forecast systems: The cost 731 action. *Atmospheric Research*, 100, 2011.

A. M. Rossa and D. Leuenberger. Sensitivity of the lhn scheme to non-rain echoes. *Meteorological Applications*, 15:503–511, 2008. doi: 10.1002/met.99.

M. Bruen M.D. Fruehwald Macpherson B. Holleman I. Michelson D. Rossa, A.. and s. Michaelides. Cost 717 action . use of radar observation in hydrology and nwp models. *Cost Meteorology*, page 286, 2005.

H.H. Schiesser, R.A. Houze, and H. Huntrieser. The mesoscale structure of severe precipitation systems in Switzerland. *Monthly Weather Review*, 123 (7):2070–2097, 1995.

C. H. Schraff. Mesoscale data assimilation and prediction of low stratus in the alpine region. *Meteor. Atmos. Phys.*, pages 21–51, 1997.

D. Sempere-Torres, G. Pegram, X. Llort, C. Velasco-Forero, and M. Franco. "real-time assessment of accuracy and quality in quantitative precipitation estimation. In *Proceedings of Fifth European Conference on Radar in Meteorology and Hydrology (ERAD2008). Helsinki (Finlandia). ISSN: 978-951-697-676-4.*, volume 4 of *ERAD Publication Series*, 2008.

K. Stephan, S. Klink, and C. Schraff. Assimilation of radar-derived rain rates into the convective-scale model cosmo-de at dwd. *Quarterly Journal of the Royal Meteorological Society*, 134(634):1315–1326, 2008. URL `http://dx.doi.org/10.1002/qj.269`.

J. Steppeler, G. Doms, U. Schättler, H.-W. Bitzer, A. Gassmann, U. Damrath, and G. Gregoric. Meso-gamma scale forecasts using the nonhydrostatic model LM. 82:75–96, 2003.

Wei-Kuo Tao, Stephen Lang, Xiping Zeng, Shoichi Shige, and Yukari Takayabu. Relating convective and stratiform rain to latent heating. *Journal of climate*, 23:1874–1893, 2009.

L. Turconi Tropeano, D. and S. Sanna. Debris flows triggered by the 29 august 2003 cloudburst in val canale, eastern italian alps. 2004.

M.P. Van Horne, E.R. Vivoni, D. Entekhabi, R.N. Hoffmann, and C. Grassotti. Evaluating the effects of image filtering in short-term radar rainfall forecasting for hydrological applications. *Meteorol. Appl.*, 2006.

M. L. Weisman and J. B. Klemp. The dependence of numerically simulated convective storms on vertical wind shear and buoyancy. *Monthly Weather Review*, 110:504–520, 1982.

M.L. Weisman, C. Davis, W. Wei, K.W. Manning, and J.B. Klemp. Experiences with 0 36 h explicit convective forecasts with the wrf-arw model. weather and forecasting. 2008.

Gao J. Brewster K. Xue, D.W. and K.K. Droegemeier. The advanced regional prediction system (arps), storm-scale numerical weather prediction and data assimilation. *Meteor. Atmos. Phys.*, 82, 2003.

Beven K.J. Bruen M. Cofino A.S. Kok K. Martin E. Nurmi P. Orfila B. Roulin E. Schroter K. Seed A. Szturc J. Vehvilinen B. Zappa, M., U. Germann, and A. Rossa. Propagation of uncertainty from observing systems and nwp into hydrological models: Cost-731 working group 2. *Atmos. Sci. Lett.*, 11, 2010.